Modelling forest management within a global vegetation model-Part 1: Model structure and general behaviour

Valentin Bellassen, G. Le Maire, Jean-Francois Dhote, Philippe Ciais, N. Viovy

Title: Modelling forest management within a global vegetation model – Part 1: model structure and general behaviour

Authors: Bellassen V[1], Le Maire G[2], Dhôte JF[3], Viovy N[1], Ciais P[1]

[1]Laboratoire des Sciences du Climat et de l'Environnement, Commissariat à l'énergie atomique / CEA-Orme des Merisiers / F-91191 Gif-sur-Yvette CEDEX / France

[2]Fonctionnement et pilotage des écosystèmes de plantations, Centre de coopération internationale en recherche agronomique pour le développement / Maison de la Télédétection - TA C-91 – MTD / 500 Rue J.F. Breton / 34093 Montpellier cedex 5 / France

[3]Direction Technique et Commerciale Bois, Office National des Forêts / Boulevard de Constance / 77300 Fontainebleau / France

Journal: Ecological Modelling

Publication year: 2010

Corresponding author: Bellassen V

Phone: +33 1 69 08 31 01

Fax: +33 1 69 08 30 73

E-mail: valentin.bellassen@lsce.ipsl.fr

12 Abstract

13 This article describes a new Forest Management Module (FMM) that explicitly simulates forest stand growth and management within a process-based global vegetation model (GVM) called ORCHIDEE. The net primary productivity simulated by ORCHIDEE is used as an input to the FMM module. The FMM then calculates stand and management characteristics such as stand density, tree size distribution, tree growth, the timing and intensity of thinnings, wood extraction and litter generated after thinning. Some of these variables are then fed back to ORCHIDEE. These computations are made possible with a distribution-based modelling of individual tree size. The model derives natural mortality from the relative density index (*rdi*), a competition index based on tree size and stand density. Based on the common forestry management principle of avoiding natural mortality, a set of rules is defined to calculate the recurrent intensity and frequency of thinning and forestry operations during the stand lifetime. The new coupled model is called ORCHIDEE-FM (Forest Management).

14 The general behaviour of ORCHIDEE-FM is analysed for a broadleaf forest in north-eastern France. Flux simulation throughout a forest rotation compare well with literature values, both in absolute values and dynamics.

15 Results from ORCHIDEE-FM highlight the impact of forest management on ecosystem C-cycling, both in terms of carbon fluxes and stocks. In particular, the average Net Ecosystem Productivity (NEP) of 225 $gC.m^{-2}.yr^{-1}$ is close to the biome average of 311 $gC.m^{-2}.yr^{-1}$. The

NEP of the “unmanaged” case is 40% lower, leading us to conclude that management explains 40% of the cumulated carbon sink over 150 years. A sensitivity analysis reveals 4 major avenues for improvement: a better determination of initial conditions, an improved allocation scheme to explain age-related decline in productivity, and an increased specificity of the self-thinning curve and the biomass-diameter allometry.

Keywords: forest management; global vegetation model; ORCHIDEE; carbon cycle

Introduction

Global Vegetation Models (GVMs) simulate the carbon, energy and water budgets of ecosystems on a grid. In their representation of forests, individual tree characteristics, and the processes which control them, are generally ignored. To some very rare exceptions (eg. Sato et al., 2007), most GVMs simulate the functioning of an “average tree” for forest ecosystems in each grid point and discard the effects of forest management.

In their global applications (eg. Sitch et al., 2008), GVMs usually calculate biomass to be in steady state equilibrium with climate. Discarding forest management has hitherto precluded a realistic estimation of biomass stocks in GVMs: the steady state assumption leads to overestimated biomass (Ciais et al., 2008), and to underestimated carbon sink due to forest re-growth (Desai et al., 2007; Schaefer et al., 2008; Carvalhais et al., 2010). A GVM intercomparison (Viovy et al., 2010) further indicates huge between-model differences for

aboveground biomass (ranging 0.5 – 10 kg C m^{-2}) simulations, illustrating the fact that GVM results are seldom evaluated against fine scale biomass data.

Replacing a forest by an average tree in a GVM raises two spatial scaling issues. The first issue is that stands of different ages coexist within the same grid point. This sub-grid heterogeneity problem can be tackled by modelling explicitly different age classes existing within each point (Zaehle et al., 2006; Shevliakova et al., 2009). The second scaling issue is that trees of different sizes coexist within the same forest stand. Forest management, which reacts in practice to the size and density of trees, is delicate to simulate in this context. For instance, Zaehle *et al.* (2006) decided in the LPJ model to remove a percentage of wood biomass in each grid point based upon a simple age criteria, based on 'top-down' timber harvest statistics only available at country scale. As a result, the carbon budget of regions where forests are intensively managed, such as Europe, cannot be confidently reproduced (Lindner et al., 2004; Zaehle et al., 2006).

Another drawback of ignoring within-stand heterogeneity in GVM is that estimates by these models are difficult to relate with the most abundant source of validation and parameterization data: plot measurements from forest inventories (Valentine and Mäkelä, 2005). Indeed, forest inventories measure variables such as tree density, basal area, or standing volume, which depend on processes that call for an explicit description of within-stand heterogeneity (Dhôte, 1999).

Intensive efforts were made to simulate vegetation dynamics and individual tree characteristics through gap models (Pacala et al., 1996; Pretzsch et al., 2002; Lischke et al., 2006) and growth and yield models (Hoffmann, 1995; Dhôte and Hervé, 2000; Masera et al., 2003). Gap models

were originally developed by ecologists to simulate species succession in a newly opened gap. They represent mortality processes at tree level (Bugmann, 2001). By contrast, growth and yield models were originally developed by foresters to predict the number and size of the stems that a stand will yield. Their representation of mortality processes focuses on emergent properties at the scale of the stand (Saint-Andre et al., 2008). Both types of models are often spatially limited by the need for a local calibration of productivity which, together with rotation length, has been shown to contribute most to simulation uncertainty at regional scale (Bottcher et al., 2008). Therefore, they both need specific adaptations to be included in GVM.

This paper describes a new forest growth and management module (FMM) that is inspired from the forest growth and yield model FAGACEES (Dhôte and Hervé, 2000). It sets focus on the characteristics of individual trees within a forest stand, and can incorporate management rules based on actual forestry operations. The FMM is designed to be portable into a GVM, but it can also be applied to yield tables data, e.g. for cross validation. The FMM can simulate clear cuts, intermediate thinnings and natural mortality due to competition (self-thinning). We have coupled the FMM to a GVM called ORCHIDEE (Krinner et al., 2005).

In the following, the structure and functioning of the FMM model and its coupling to ORCHIDEE are described. Test simulations are performed for a virtual broadleaf forest in North-eastern France in order to illustrate the general response of ORCHIDEE-FM, and to assess the differences between ORCHIDEE-FM and the standard version of the ORCHIDEE GVM which simulates equilibrium biomass levels in unmanaged forests. For the ORCHIDEE-FM simulations, we consider an “unmanaged” scenario and a “managed” scenario. The expected improvements

are benchmarked using carbon stocks, carbon fluxes, and stand characteristics. The sensitivity of the ORCHIDEE-FM model to varying parameters values is evaluated. Obviously, a single example site offers an illustration of the behaviour of the FMM, but does not constitute a rigorous assessment of model performance. A follow-up paper (Bellassen et al., Part 2, this issue) presents the validation of ORCHIDEE-FM against a variety of stand-scale and continental-scale datasets provided by forest inventories, yield tables and permanent monitoring plots.

20 Model structure

20.1 Modelling strategy

Management processes can be modelled at different levels of complexity. Most often in GVMs, a constant proportion of standing biomass is simply removed from the system (Zaehle et al., 2006). Franklin et al. (2009) establish a synthetic set of equations averaging management processes, with the explicit objective of being easily added to GVMs. At a higher level of complexity, Moorcroft et al. (2001) and Sato et al. (2007) represent the evolution of each tree crown on a daily time-step, which enables them to compute photosynthesis and mortality at the tree scale. In this continuum, we opted for an intermediate level of complexity. As Sato et al. (2007), we compute the distribution of individual tree characteristics such as circumference and height, and use this information to simulate stand-scale mortality and the repartition of stand-scale growth among individual trees. We therefore move from the “average tree” modelling strategy of Zaehle et al. (2006) to an “average stand” modelling strategy similar to Desai et al. (2007). Trees of different sizes are simulated within each grid cell, and their

evolution from an initial size distribution represents the average stand composition in the cell for a series of stand ages. This fine-scale representation allows an easy comparison to real tree stands, as well as useful information for upcoming developments on wood products and physical interactions of forests with the atmosphere. Though desirable, a process-based tree-scale computation of photosynthesis and mortality is currently incompatible with the computing constraints of half-hourly flux simulation in a fully coupled Earth System Model such as IPSL-CM4 (Marti et al., 2010).

The management module (FMM) provides an explicit description of the characteristics (basal area and height) of each tree in an "average hectare", representative of a given age-class at the resolution at which ORCHIDEE operates (typically 10-50 km² to allow for regional to global simulations). In Europe, even-aged high forests are the most common forest type (Vetter et al., 2005; Vallet et al., 2006), and their management is generally aimed at avoiding natural mortality from competition by selectively felling trees (Nabuurs et al., 2002). This is the default type of forest management simulated by the FMM, although its simulation of self-thinning and clear cutting makes it applicable to other regions by disengaging the "intermediate thinning" option.

The FMM is inspired from an existing forestry model, FAGACEES (Dhôte and Hervé, 2000). All the equations of the FMM, be they adapted from FAGACEES or not, are fully described below.

20.2 Structure of the ORCHIDEE Global Vegetation Model

20.2.1 Standard structure of ORCHIDEE

The ORCHIDEE global vegetation model ("ORganizing Carbon and Hydrology In Dynamic Ecosystems") is designed to operate from regional to global scales (Krinner et al., 2005). It is a process-driven model, composed of two main components

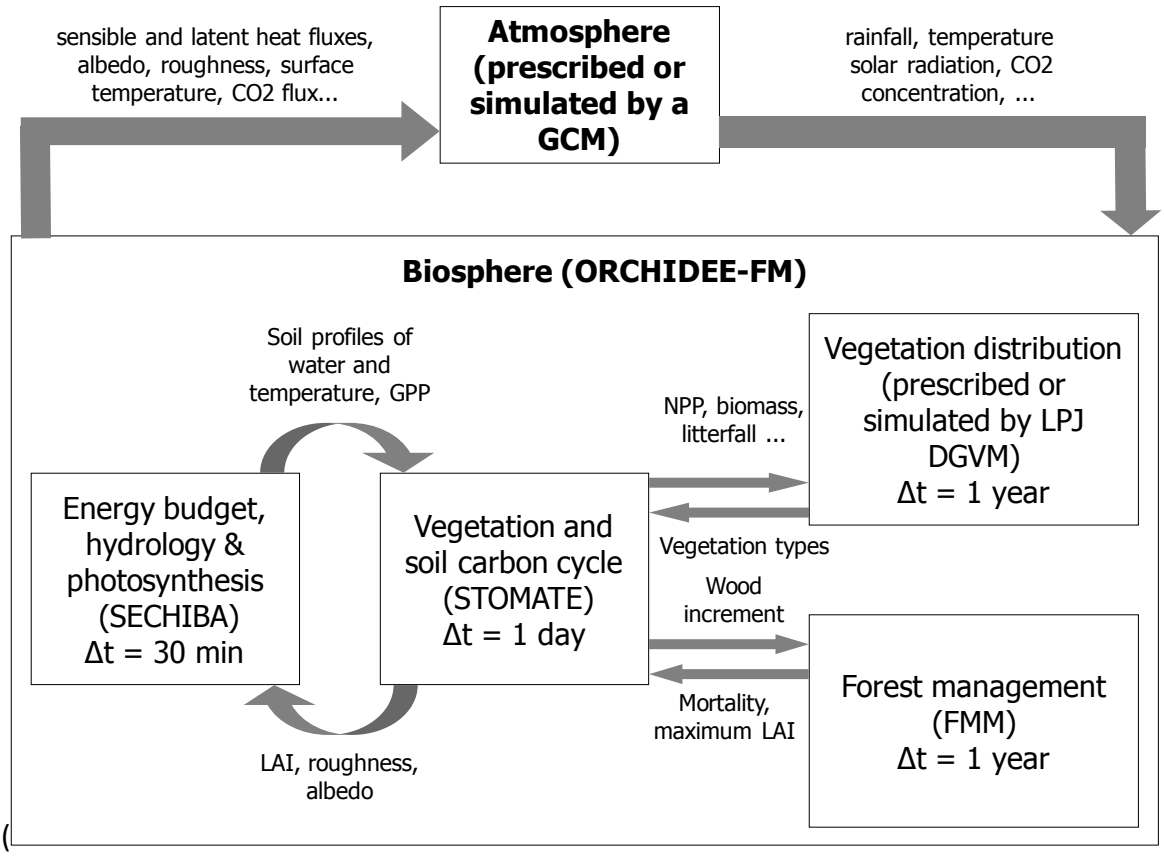

(

Figure 1). SECHIBA computes the energy and hydrology budget on a half-hourly basis, together with the gross primary production (GPP). These results are fed to STOMATE, the carbon cycle component. STOMATE simulates the carbon cycle on a daily basis: GPP is allocated to the different organs, and then respired by the plant or by soil micro-organisms when parts of the

148 plant die. These processes determine several stand-scale characteristics such as leaf area index
149 (LAI) and canopy roughness, which are fed back to SECHIBA as they impact the energy and
150 water budget. The equations of ORCHIDEE are given by Ducoudre et al. (1993), Krinner et al.
151 (2005) and in http://orchidee.ipsl.jussieu.fr/.
152 ORCHIDEE requires seven climatic driving variables on a half-hourly timescale: air temperature,
153 precipitation, specific humidity, wind speed, pressure, short wave and long wave incoming
154 radiation. Other pedo-climatic inputs such as CO_2 concentration, soil water holding capacity,
155 and soil texture are used at lower time-resolutions. The meteorological variables can be
156 prescribed from climate datasets in so-called "offline" simulations. But ORCHIDEE can also be
157 dynamically linked to the atmosphere and ocean components of the IPSL-CM4 earth system
158 model (Marti et al., 2010) in so-called "online" simulations.
159 As in most global biogeochemical models, the vegetation is classified into Plant Functional
160 Types (PFT), with 13 different PFT over the globe. Distinct PFTs follow the same set of governing
161 equations, but with different parameter values, except for the calculation of the growing
162 season onset and termination, which involve PFT-specific processes (Botta et al., 2000). Only
163 the European woody PFTs (temperate needleleaf evergreen, temperate broadleaf evergreen,
164 temperate broadleaf summergreen, boreal needleleaf evergreen, boreal broadleaf
165 summergreen and boreal needleleaf summergreen) are of interest for this study.

166 ### 20.2.2 Specific add-ons to the standard version

167 Explicit modelling of forest stand growth and management within the ORCHIDEE framework
168 could not be achieved without the addition of several processes to the standard version: age-

related decline in net primary production (NPP), age-related limitation of LAI in young stands, age-related allocation ratio between stem and coarse roots, branch mortality and a coarse woody debris litter compartment.

Age-related decline in NPP

NPP has long been shown to decline in older forest stands, even if the processes underlying this decline are still subject to controversy (Gower et al., 1996; Magnani et al., 2000; Murty and McMurtrie, 2000; Lefsky et al., 2005). Three main hypothesis have been laid out to explain this phenomenon: an increase of autotrophic respiration as the tree gets bigger, a decrease of nitrogen availability from the initial litter input of tree fall or harvest residues, and hydraulic constraints on photosynthesis efficiency (Gower et al., 1996; Ryan et al., 2006). The first process is already represented in ORCHIDEE but is not sufficient to simulate a decrease of NPP with age. The two other processes were empirically added to ORCHIDEE through the introduction of a new limiting factor to photosynthesis efficiency, $decl_{factor}$ Eq. (1).

$$\left(\begin{array}{l} \text{If } age_{stand} > decl_{start}: \quad Vmax = decl_{factor} \times Vmax_{std} \\ \text{And}: \quad decl_{factor} = \max\left(decl_{max}, \frac{age_{stand} - decl_{start}}{decl_{end} - decl_{start}} \right) \end{array} \right) \quad \textbf{(1)}$$

where *Vmax* is the photosynthesis efficiency, $decl_{factor}$ is the age-related decline factor, $Vmax_{std}$ is the standard value of *Vmax* in ORCHIDEE, age_{stand} is the age of the stand, $decl_{max}$ is the maximum age-related decline factor, $decl_{start}$ is the age at which age-related decline starts and $decl_{end}$ is the age at which age-related decline ends.

187 The age-dependency of $decl_{factor}$ was calibrated on the age-related decline of aboveground
188 wood increment from a database of European yield tables (JRC, 2009, see appendix 7.1 for
189 details).

190 *Age-related limitation of LAI in young stands*

191 ORCHIDEE is highly dependent on a PFT-specific parameter setting the maximal LAI value
192 (lai_{max}) that a PFT can reach (Jung et al., 2007). As the creation of new leaves is time and energy
193 consuming, and because structural constraints do not always allow young trees to close the
194 canopy, stand LAI in forests does not reach its maximum value before 10-15 years (Ovington
195 and Madgwick, 1957; Vieira et al., 2003; Hurtt et al., 2004). This process is negligible for the
196 standard version of ORCHIDEE which represents a steady-state equilibrium, but gets important
197 in ORCHIDEE-FM where early stand development stages are also simulated. Therefore, lai_{max} is
198 made dependant on age during the first years Eq. (2):

$$\mathrm{lai}_{\max} = \mathrm{lai}_{\max\_\mathrm{std}} \times \min\left(\sqrt{\frac{\mathrm{age}_{\mathrm{stand}}}{15}}, 1\right) \quad (2)$$

199

200 where lai_{max} and lai_{max_std} are the maximal LAI value in $m^2\ m^{-2}$ in respectively ORCHIDEE-FM and
201 the standard version of ORCHIDEE and age_{stand} is the age of the stand in years.

202 *Age-related allocation ratio between stem and coarse roots*

203 The root/shoot ratio of trees has been shown to decrease with age (Mokany et al., 2006). The
204 introduction of age in ORCHIDEE-FM allows simulating this pattern by decreasing the
205 belowground-to-aboveground-wood allocation ratio with age Eq. (3):

$$\frac{\text{alloc}_{ab}}{\text{alloc}_{be}} = \text{alloc}_{min} + (\text{alloc}_{max} - \text{alloc}_{min}) \times \left(1 - e^{-\frac{\text{age}_{stand}}{\text{demi}_{alloc}}}\right) \quad \textbf{(3)}$$

where $alloc_{ab}$ and $alloc_{be}$ are respectively the allocation to aboveground and belowground sapwood in gC m^{-2}, $alloc_{min}$, $alloc_{max}$, and $demi_{alloc}$, are the minimum, maximum, and half-life of the aboveground/belowground sapwood allocation ratio and age_{stand} is the age of the stand in years.

Moreover, the allocation to fruits, set at 10% of NPP by Krinner et al. (2005) was reverted to 0.5%, a value more consistent with field estimates (Granier et al., 2008).

Branch mortality

Branches are usually not harvested (IFN, 2006), although the rising demand for biomass may change this in the future (European Commission, 2005). In the perspective of coupling ORCHIDEE with a forest management module, it is thus necessary to differentiate stem and branches within the aboveground biomass compartment. This is done by setting a constant PFT-specific branch/stem ratio ($branch_{ratio}$) and a constant sapwood/heartwood ratio in branches ($branch_{sap/heart}$). Two processes can lead to branch mortality: branch turnover as the tree grows, and tree mortality due to thinning (natural or anthropogenic). Since branch turnover is only one of the two processes driving branch mortality in our model, we set the branch turnover rate ($branch_{turn}$) toward the lower end of the 0.02-0.05 $year^{-1}$ range of literature values for other models (Lloyd and Farquhar, 1996; Masera et al., 2003).

Coarse woody litter compartment

Litter and soil carbon dynamics in the standard version of ORCHIDEE are derived from an older version of the CENTURY model (Parton et al., 1988). As it was designed for grasslands, this version of CENTURY only has two litter compartments: structural and metabolic. The structural compartment represents the stalk of herbaceous vegetation that decomposes fairly rapidly compared to woody debris. In the standard version of ORCHIDEE at steady state, this leads to an underestimation of the litter pool but has little impact on fluxes as the woody litter input is almost constant over time. This impact is much stronger when the forest management module (FMM) is activated, as woody litter inputs are irregular and potentially large: if only a few stems die after a self-thinning event, all branches and coarse roots are laid off to the decomposing woody litter pool. It was thus necessary to add a coarse woody litter compartment which decomposes more slowly (Lloyd and Farquhar, 1996), with a maximum turnover rate (τ_{cwd}) set lower than the 4.08 $year^{-1}$ of structural litter. Due to moisture, temperature and lignin content limitations however, the actual turnover rate is much lower than its theoretical maximum of 0.75 $year^{-1}$ (Table 1), averaging 0.03 $year^{-1}$ for coarse woody debris. This value is consistent with observed and simulated residence time of around 30 years (Olsson et al., 1996; Schelhaas et al., 2004; Nagy et al., 2006).

20.3 Structure of the forest management module (FMM)

20.3.1 General structure

The general structure of the FMM, represented in Figure 2, is inspired from the FAGACEES stand-level model (Dhôte and Hervé, 2000). The FMM runs on an annual time-step, can be coupled to ORCHIDEE, and simulates three main processes: the annual distribution of cumulated stand wood increment to individual trees, the natural mortality due to self-thinning, and the timing and intensity of intermediate thinnings or clear cuts.

20.3.2 Individual growth of trees

The first step of the FMM is to allocate the yearly wood increment calculated by ORCHIDEE to a population of individual trees, here described by the distribution of their circumferences.

Initial distribution of tree circumferences

After a clear cut, the initial circumference distribution has to be prescribed. The initial number of trees is set to a default $n_{maxtrees}$ and the initial distribution of circumferences follows a truncated exponential law of parameter λ (Lanier, 1994; Dhôte and Le Moguédec, 2003):

$$\lambda = \frac{\sqrt{2}}{\pi \times \mathrm{Dg}_{\mathrm{init}}} \quad \textbf{(4)}$$

where the parameter Dg_{init} is the initial quadratic mean diameter.

Details on the algorithm producing the exponential distribution are given in appendix 25.2.

Allocation of stand-level wood increment to individual trees

To simulate competition for resources – such as light, water and nutrients – between trees, and the resulting heterogeneity in tree diameters, larger trees are assumed to grow faster in basal area (Ryan et al., 2006). The individual growth function (Eq. 5) is taken from Deleuze (2004):

$$\delta ba_i = \frac{\gamma}{2} \times \left(circ_i - m\sigma + \sqrt{(m\sigma + circ_i)^2 - 4\sigma \times circ_i} \right) \quad (5)$$

where δba_i is the annual increase in basal area of tree *i* in square meters, $circ_i$ is the circumference of tree *i* in meters. γ, σ and *m* are respectively the slope, threshold and smoothing parameters (see Figure 3): trees whose circumference is lower than σ barely grow, γ is the slope of the δba_i vs $circ_i$ relationship above σ.

σ is a function of tree density within the stand, calibrated with data from permanent monitoring plots (Dhôte and Hervé, 2000).

$$\ln(\sigma) = a_\sigma \times \ln(circ_{med}) + b_\sigma \quad (6)$$

where $circ_{med}$ is the median circumference of trees in meters, and a_σ and b_σ are parameters. The main conceptual difference between the FMM and FAGACEES comes from how γ and σ are computed. In FAGACEES, γ represents intersite variability in stand-level growth increment and is therefore calibrated on a site-per-site basis. σ is then adjusted so that the individual circumference growths computed by Eq. (5) are consistent with total stand growth. In ORCHIDEE-FM however, the inter-site variability in stand-level growth increment is computed by ORCHIDEE. The FMM estimates σ from the median circumference from Eq. (6), and then

277 computes *γ* so that the individual circumference increments computed by Eq. (5) are consistent
278 with the ORCHIDEE-prescribed stand woody growth. The site-by-site adjustment of *γ* is
279 therefore done by iteratively computing a value of *γ* that yields exactly the aboveground wood
280 increment given by ORCHIDEE (*σ* and *m* being fixed). Solving for *γ* requires a tree level biomass-
281 circumference allometry relationship, given by Eq. (7) (Zianis and Mencuccini, 2004):

$$\text{biomass}_i = a_{bc} \times \text{circ}_i^{\,b_{bc}} \quad (7)$$

282

283 where $biomass_i$ is the dry aboveground biomass of tree *i* in kg and $circ_i$ is the circumference of
284 tree *i* in centimetres.

285 ### 20.3.3 Self-thinning curves

286 *Self-thinning curves and natural mortality*

287 Natural mortality processes in forest stands have been studied for a long time. The FMM uses
288 the well-established Reineke rule to test whether self-thinning occurs (Eq. 8). It happens when
289 stand density exceeds the maximum density corresponding to its quadratic mean diameter
290 (Reineke, 1933).

$$\text{dens}_{max} = \frac{\alpha_{st}}{Dg^{\beta_{st}}} \quad (8)$$

291

292 where $dens_{max}$ is stand maximum density in ind ha^{-1} (individuals per hectare), α_{st} and β_{st} are
293 parameters, and *Dg* is the quadratic mean diameter (Eq. 9) in m.

$$Dg = \sqrt{\frac{\sum_i diam_i^2}{dens}} \quad (9)$$

where $diam_i$ is the diameter of tree i in m and $dens$ is the actual density of the stand. Yang et al. (2002) showed that these relationships were not dependent on site quality, but could vary between species. This argues for a PFT-specific parameterization of Eq. (8).

Relative density index (rdi) and anthropogenic thinning

When the stand has reached a high enough dominant height – defined as the average height of the 100 tallest trees per hectare – h_{start}, human intervention through commercial thinning becomes feasible (Lanier, 1994; Grote and Erhard, 1999). In order to test this condition, the height of each tree is estimated from an allometric relationship. From the five allometric relations analysed by Newton and Amponsah (2007), a model of intermediate complexity was chosen and calibrated on data from the French national forest inventory (IFN, 2008):

$$height_i = 1.3 \times \alpha \times ba_j^{\chi} \times \left(1 - \exp\left(-\delta \times dens_j^{\varphi} \times \frac{100}{2\pi} circ_i\right)^{\varphi}\right) \quad (10)$$

where $height_i$ and $circ_i$ are respectively the height and circumference of tree i in meters, and ba_j and $dens_j$ are the basal area and tree density of the stand, respectively in $m^2\ ha^{-1}$ and $ind\ ha^{-1}$. α, χ, δ, Φ, and φ are parameters. Details on calibration are given in appendix 25.3.

Then, in order to avoid natural mortality and maximize wood exploitations, foresters are assumed to remove trees from the stand by thinning, in order to maintain a lower density than

311 $dens_{max}$. To simulate this behaviour, we define the relative density index (*rdi*) as the ratio of
312 actual to maximal density Eq. (11).

$$\mathrm{rdi} = \frac{\mathrm{dens}}{\mathrm{dens}_{\max}} \quad \textbf{(11)}$$

313

314 where *rdi* is the relative density index, and *dens* and $dens_{max}$ are respectively the actual and
315 maximal tree density of the stand in ind ha^{-1}.
316 Throughout the rotation, *rdi* is kept close to a targeted value rdi_{target} that depends on
317 management practices: the lower the rdi_{target}, the more intensive the management and the
318 lower the stand density. *δrdi* determines the leeway allowed around rdi_{target}: when *rdi* reaches
319 rdi_{target} + *δrdi*, the stand is thinned until it is scaled back to rdi_{target} – *δrdi* (see Figure 3). The final
320 harvest occurs when stand density falls below $dens_{target}$ or when stand age reaches age_{target}
321 (Lanier, 1994).

322 **20.3.4 Harvest**

323 *Tree removal*

324 In order to determine which trees are felled during a thinning event, a probability of death τ_i is
325 attributed to each tree Eq. (12). A felling algorithm is then applied so that the *rdi* gets back to 1
326 (self-thinning) or rdi_{target} – *δrdi* (anthropogenic thinning) while respecting the tree-level
327 probability of death τ_i.

$$\left(\begin{array}{l} \text{If } th_{strat} \geq 0\text{: } \tau_i = \tau_{min} + (\tau_{max} - \tau_{min}) \times \left(\dfrac{circ_{max} - circ_i}{circ_{max} - circ_{min}} \right)^{th_{strat}} \\ \\ \text{If } th_{strat} < 0\text{: } \tau_i = \tau_{min} + (\tau_{max} - \tau_{min}) \times \left(\dfrac{circ_i - circ_{min}}{circ_{max} - circ_{min}} \right)^{|th_{strat}|} \end{array} \right) \quad \textbf{(12)}$$

where τ_i and $circ_i$ are probability of death and the circumference of tree *i* in meters, $circ_{min}$ and $circ_{max}$ are the minimum and maximum circumference in the stand in meters, and τ_{min} and τ_{max} are respectively the minimum and maximum probabilities of death.

The value of the parameter th_{strat} sets the thinning strategy: if $th_{strat} > 0$, a "thinning from below" strategy is simulated, with smaller trees preferentially thinned to obtain larger logs in the future. If $th_{strat} < 0$, a "thinning from above" strategy is simulated, with larger trees preferentially thinned thus freeing resources for smaller trees (for an illustration of this range of possible thinning strategies, see appendix 25.4).

Final harvest

Final harvest occurs at age_{target} or if a thinning event is predicted when stand density is below $dens_{target}$. All trees are cut and a new stand begins to grow in order to simulate multiple rotations over long time periods. Stems are exported while branches and coarse roots move to the litter pool as coarse woody debris. All leaves and fine roots go to the structural and metabolic litter pools, following the standard proportions set by ORCHIDEE.

20.4 Coupling: interaction between wood increment and forest management

The only input from ORCHIDEE to the FMM is the mean annual stand-level wood increment, allocated in the different biomass compartments (aboveground vs belowground, sapwood vs heartwood vs carbohydrate reserves).

The FMM feeds back three variables to ORCHIDEE: LAI, biomass and litter (see

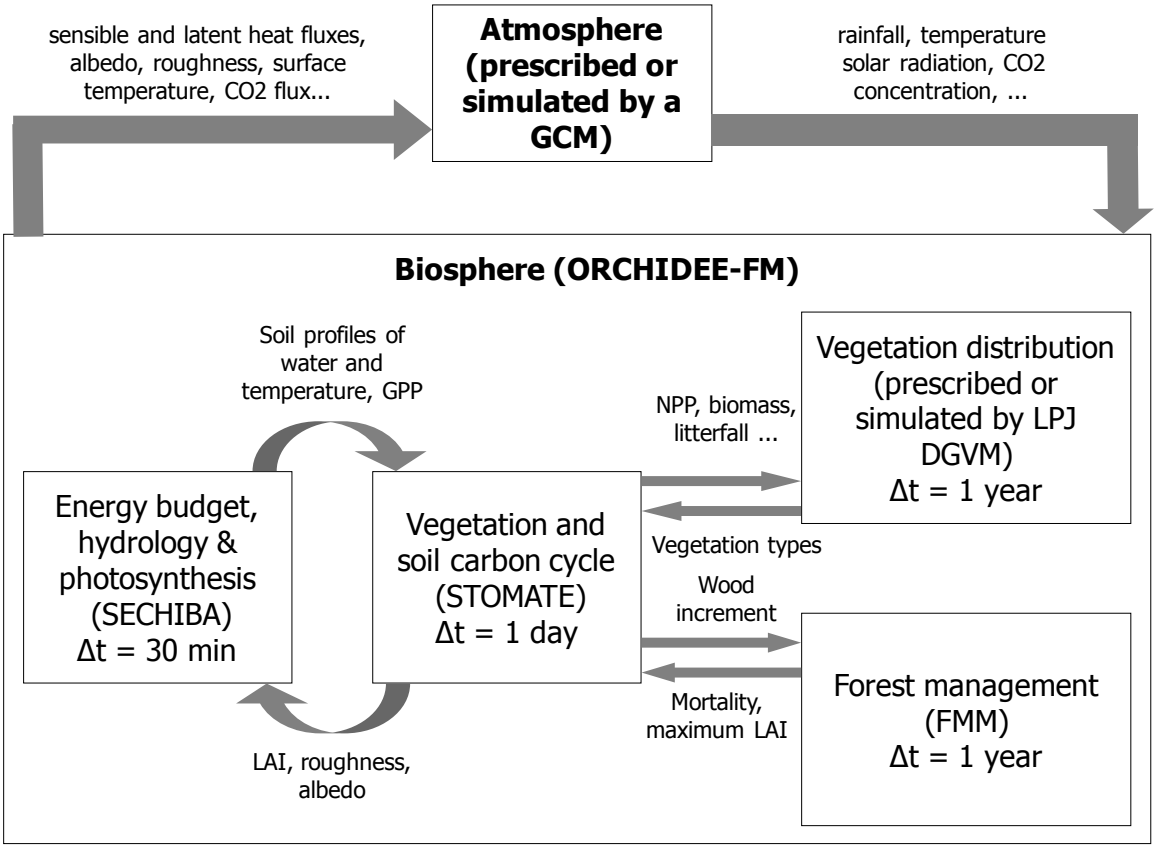

Figure 1). The soil carbon budget is indirectly impacted by the explicit simulation of branch and tree mortality in the FMM as living biomass turns – abruptly in the case of clearcuts and anthropogenic thinnings – into litter.

353 *Feedback of the FMM on the leaf area index (LAI)*

354 The stand-level LAI is modified by the FMM in two cases: when trees are too young to close the
355 canopy (see part 20.2.2), and after a thinning event. Thinnings have been shown to temporarily
356 decrease the maximum value that LAI can reach (lai_{max}), until growing branches fill the gaps.
357 When the FMM predicts a thinning event, lai_{max} is decreased by a fixed proportion δlai_{max}, and
358 recovers gradually within 3 years (Le Dantec et al., 2000; Bouriaud, 2003; Vesala et al., 2005).
359 This evolution of LAI is displayed in

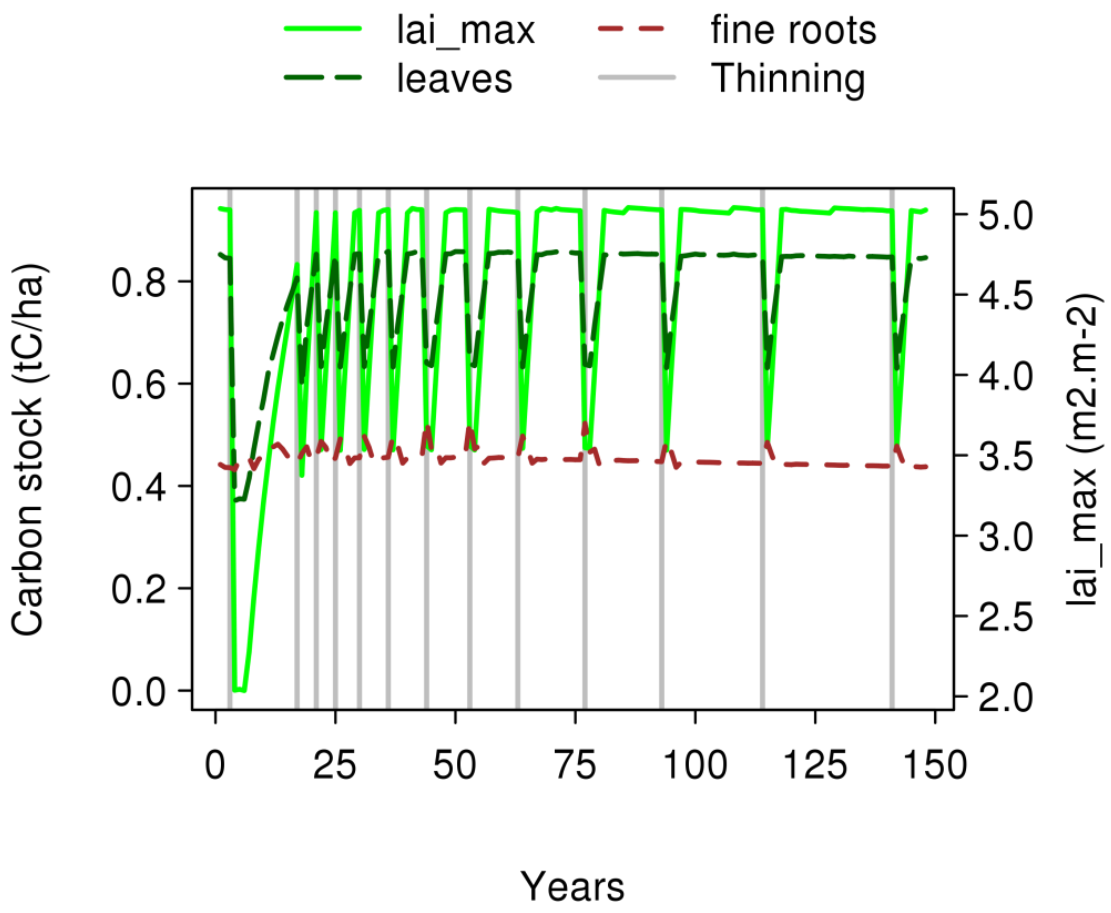

360

361 Figure 4.

Feedback of the FMM on biomass and litter

As detailed in part 20.3.4, the thinnings and final harvests simulated by the FMM have three types of impacts on the biomass which is fed back to ORCHIDEE:

- When self-thinning occurs, all biomass corresponding to the thinned individuals goes to the litter compartments.
- When anthropogenic thinning occurs, the stems of the thinned individuals are extracted from the stand, while the rest of their biomass (branches, roots, foliage) goes to litter compartments.
- During final harvest, all stems are exported out of the stand whereas branches, roots and foliage go to the litter pool. To close the carbon budget in simulations, the biomass corresponding to the initial circumference distribution is deducted from the old stand before harvest and allocated to the new one.

These feedbacks on biomass impact NPP as autotrophic respiration decreases. The resulting effect of the simultaneous decreases in GPP and autotrophic respiration after thinning will be discussed in the results part.

20.5 Parameterization

Most parameters are derived from literature, and empirical studies are preferred to modelling studies where available. Parameters for which values are available and different for broadleaves and coniferous are attributed PFT-specific values (Table 1). When the literature does not provide precise values, the French National Forest Inventory dataset (IFN, 2008) and a compilation of European yield tables (JRC, 2009) are used for calibration. The values of all

parameters specific to this version of ORCHIDEE and its associated FMM, together with their source, are summarized in Table 1.

20.6 Simulations

Three simulation set-ups are used to illustrate the impact of the FMM on the long term dynamics of carbon stocks and fluxes within the ORCHIDEE-FM framework. The first one is a control simulation using ORCHIDEE without the FMM (ORCH-STD). For the two others, the FMM is activated. In the "unmanaged case" (ORCH-FM_u), anthropogenic thinning is disabled and only self-thinning occurs. In the "managed case" (ORCH-FM_m), the full version of ORCHIDEE-FM is used.

This last set-up is also used for a sensitivity analysis of 16 key parameters. One after another (OAT approach), parameters are increased by 50% and decreased by 50%. These variations are not intended to represent a realistic range of variation or error in the parameters, but to test the response of the model to a strong variation in individual parameters.

We selected a grid cell near Nancy (48.125°N7.125°E) and a plant functional type (temperate broadleaf) for which the standard version of ORCHIDEE has already been validated (Loustau, 2004). To facilitate the interpretation of carbon dynamics, we use a single year of climate that is repeated over one rotation (approx. 150 years). The selected year was 1997, close to average climate of the grid cell in terms of temperature and precipitation. Climate data comes from the 0.25° resolution REMO reanalysis (Kalnay et al., 1996; Vetter et al., 2008). CO_2 concentration is set at 380 ppm.

A model “spinup” is performed before any simulation to define the initial state of carbon and water pools. For both the “managed” and “unmanaged” case, this “spinup” consists of repeatedly running ORCHIDEE-FM for the climate of year 1997 and a CO_2 concentration of 380 ppm until all ecosystem carbon and water pools reach cyclical steady state equilibrium (see appendix 25.5 for details). The conditions of the stand before the last clearcut are used as initial conditions, and the simulation begins with a clearcut. For the control case, the “spinup” is a repeated run of the standard version of ORCHIDEE instead of ORCHIDEE-FM.

21 Results

21.1 Stand-scale results

21.1.1 Carbon stocks

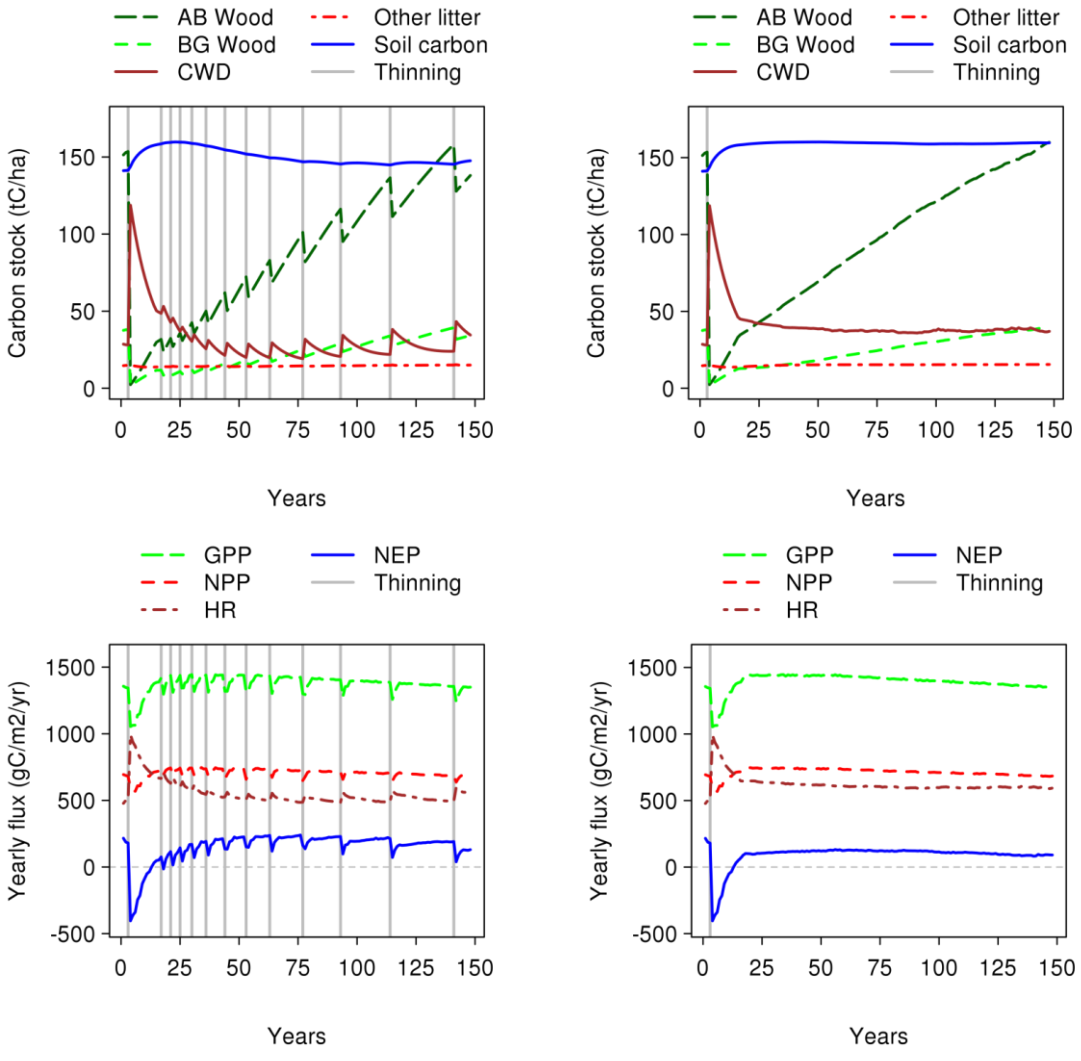

a. "Managed" case (ORCH-FM$_m$) b. "Unmanaged" case (ORCH-FM$_u$)

Figure 5 shows the evolution of the different carbon pools during a rotation. The first year clear cut of the preceding rotation puts almost all the 30 tC ha^{-1} of belowground wood and roughly a

third of the 150 tC ha^{-1} of aboveground wood into litter as coarse woody debris (CWD). The decomposition of this CWD litter drives the slow initial increase in soil carbon towards 160 tC ha^{-1}. Then, as trees grow, woody biomass follows a steadily increasing trend punctuated by temporary drops after each thinning. As the initial source of litter inputs diminishes, soil carbon peaks around year 20, and then decreases. In the "unmanaged case", where only self-thinning is allowed

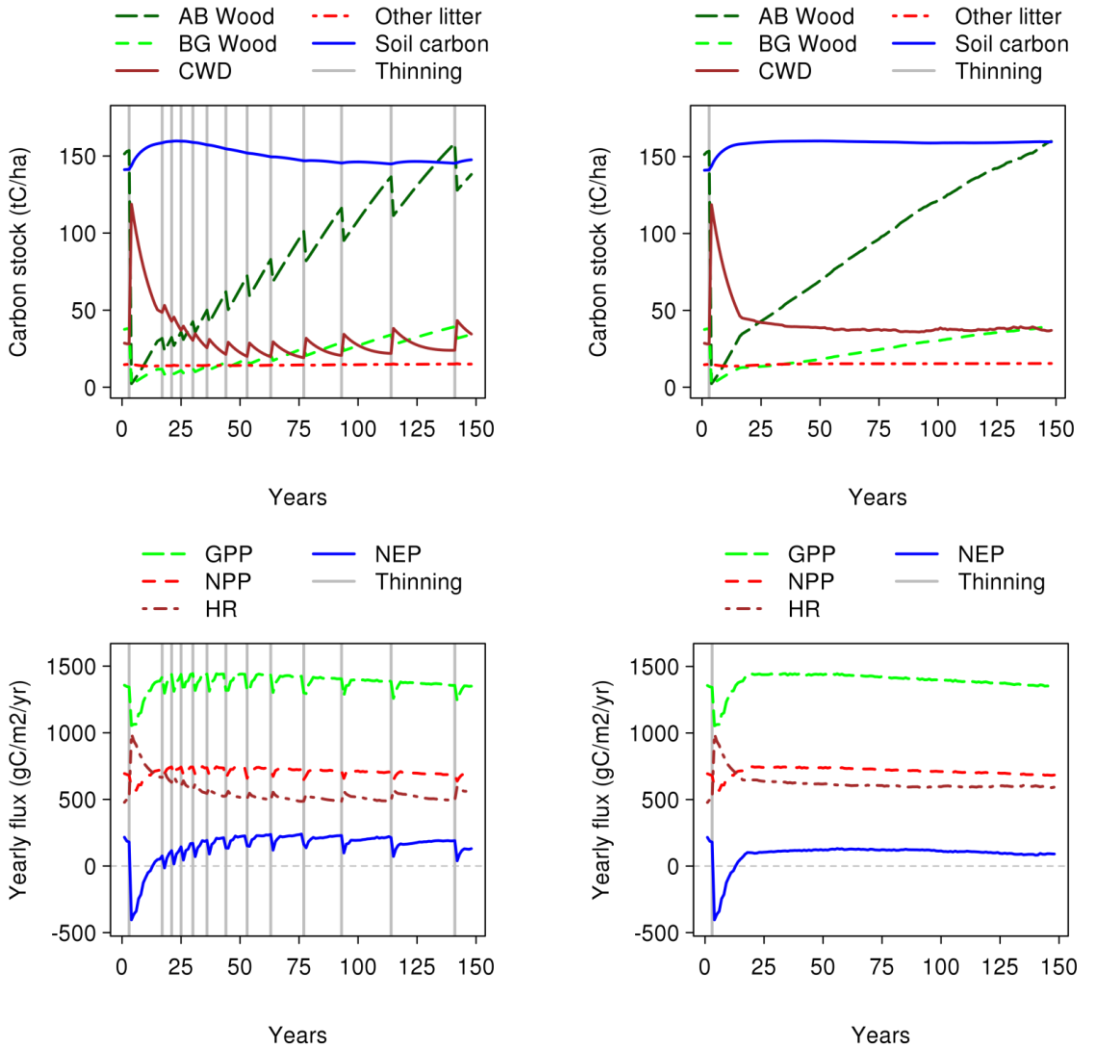

a. "Managed" case (ORCH-FM_m) b. "Unmanaged" case (ORCH-FM_u)

(

423 Figure 5), the evolution of most stocks is similar, though smoothed as they do not undergo the
424 periodic disturbance of anthropogenic thinning. Two exceptions are CWD and soil carbon which
425 keep being fed by non-exported dead stems, and reach a different equilibrium.
426 Figure 6b shows that above-ground biomass is only slightly lower (-10 tC ha^{-1} on average) when
427 the forest is regularly thinned. The main difference between the "managed" (ORCH-FM_m) and
428 "unmanaged" (ORCH-FM_u) cases in terms of biomass is seen in the coarse woody debris
429 compartment which, continuously fed by dying trees in the unmanaged case, is 10-20 tC ha^{-1}
430 higher. The comparison with the control (Figure 6a) highlights the 30% lower value of soil
431 carbon under management. The aboveground biomass catches up with the control value
432 towards the end of the rotation, after around 130 years.

21.1.2 Carbon fluxes

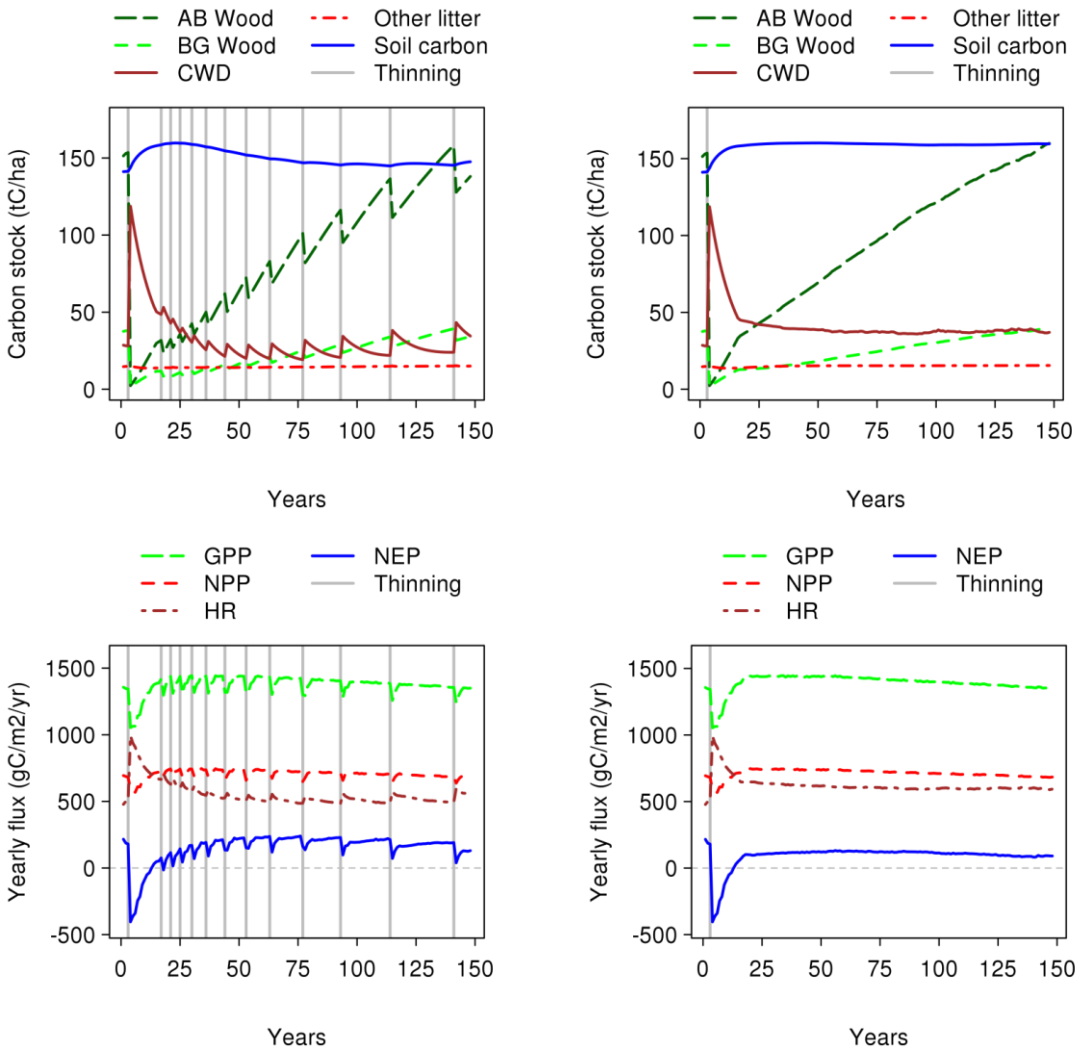

a. "Managed" case (ORCH-FM$_m$) b. "Unmanaged" case (ORCH-FM$_u$)

Figure 5 illustrates how the different carbon fluxes are affected by forest management. In the "anthropogenic thinning" case, gross primary production (GPP) and net primary production (NPP) are increasing progressively to reach 1 450 gC m^{-2} yr^{-1} and 700 gC m^{-2} yr^{-1} respectively

438 during the first 15 years, together with a gradual increase in LAI

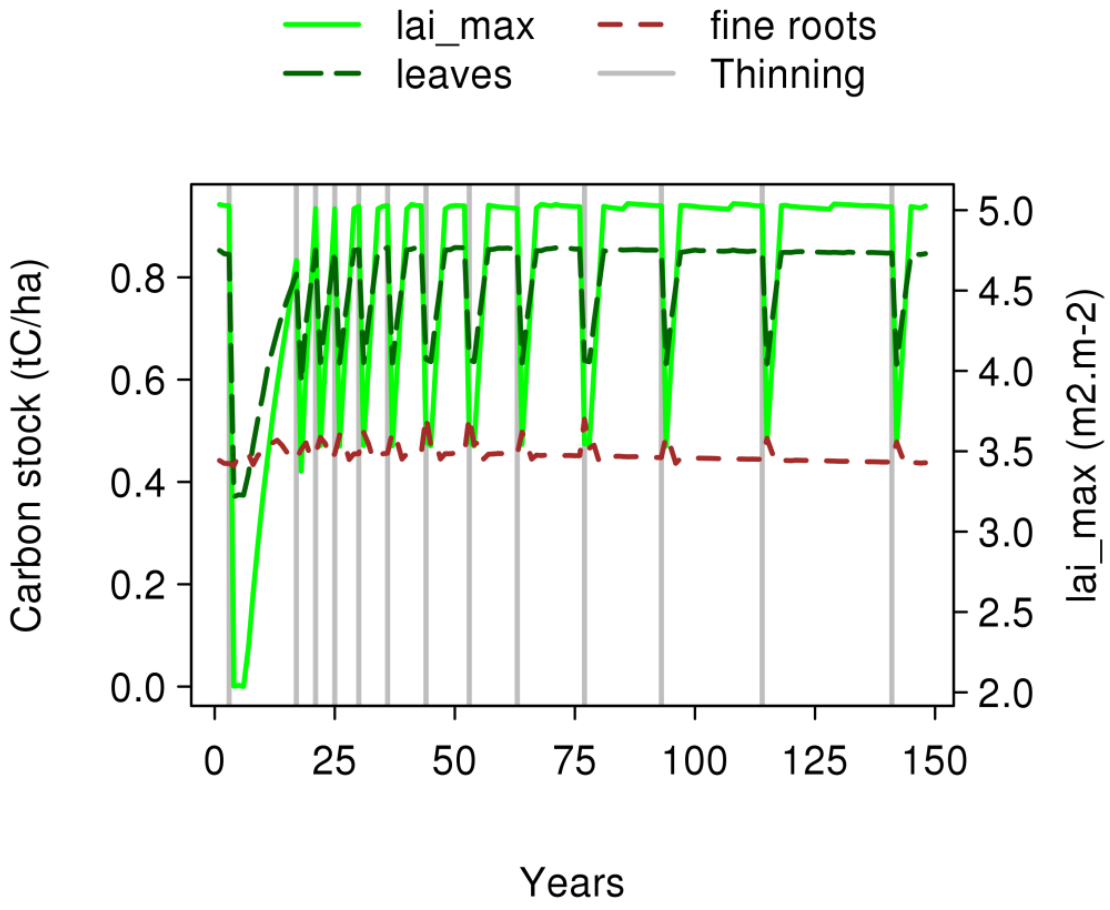

439 (

440 Figure 4). After 50 years, the age-related decline of photosynthesis efficiency weighs on GPP

441 and NPP, both of which slowly decline by 7-9%. Heterotrophic respiration (HR) displays a strong

442 peak close to 1 000 gC m^{-2} yr^{-1}, almost twice the level of its long-term average of 500 gC m^{-2} yr^{-1}.

443 This peak is due to the slash inputs from the clear cut which ends the previous rotation, as all

444 branch and belowground biomass is turned into litter. For the rest of the rotation,

445 heterotrophic respiration follows a slightly decreasing trend as the coarse woody debris

446 compartment is fed by anthropogenic thinnings. Net ecosystem productivity sums up these

447 evolutions: starting with an all-time low (source of CO_2 to the atmosphere) at -400 gC m^{-2} yr^{-1}, it
448 becomes positive (sink) after 10-15 years, peaks at 225 gC m^{-2} yr^{-1} and starts to decrease after
449 50 years as NPP decreases while HR increases.
450 Compared to an "unmanaged" scenario (Figure 6b), the main differences lie in GPP and HR. In
451 the self-thinning scenario, GPP is smoother, without the small post-thinning decreases, and HR
452 is kept higher as no exported stem is removed from litter inputs. This explains the consistently
453 higher NEP in the managed case. The comparison between the managed case and the control
454 (Figure 6a) highlights the influence of age-related decline of GPP and NPP in the FMM
455 compared to the standard ageless version of ORCHIDEE.
456 The age-related decline in NPP leads to a parallel decline in wood increment. A similar pattern is
457 observed on neighbouring national inventory plots, although the age-related decline in wood
458 increment starts earlier in the model (Figure 7).

459 ### 21.1.3 Stand characteristics

460 Table 2 gives the stand characteristics simulated by the model in the "managed scenario"
461 (ORCH-FM_m). The prescribed initial density of 10 000 trees.ha^{-1} is already reduced to 4 100
462 trees.ha^{-1} after 20 years, and continues to decrease towards 150 trees.ha^{-1} after 140 years.
463 Basal area, standing volume, and average height all keep increasing as the stand ages, though
464 the increase is faster during younger ages. The exported volume to total volume produced ratio
465 increases rapidly with the first thinnings to reach 0.55 in the long term. The time interval
466 between two thinnings also increases over time from 4 years after 20 years, up to 27 years
467 around the end of the rotation. Finally, as the stand ages, the average circumference gets closer

to the circumference of the largest tree in the stand, reflecting the progressive change in circumference distribution (see 21.2 and appendix 25.6). All these values are within the ranges given by yield tables (JRC, 2009).

21.2 Tree-scale results: distribution in circumference classes

Figure 8 shows the evolution of tree circumference. The difference between before and after thinning distributions illustrates the thinning processes whereby smaller trees are preferentially thinned. As the stand ages, the circumference distribution shifts from a decreasing exponential with a majority of smaller trees towards a majority of larger trees. This is consistent with the evolution described by the local forestry guide for this type of management (Asael, 1999).

21.3 Sensitivity analysis

The sensitivity of stand variables to a selected set of parameters is illustrated in Figure 9. The parameters listed on the left are increased by 50% (upper part of the figure) or decreased by 50% (lower part of the figure). The model is shown to be little sensitive to the initial distribution ($dens_{init}$, $circ\_init_{min}$, p_{max}). The most sensitive parameters are the ones dealing with the relative density index (σ, rdi_{lim}, rdi_{target}, and $selfth_{curve}$). Most variables are also very sensitive to allometric equations, and in particular the allometry between circumference and biomass Eq. (7).

22 Discussion

22.1 Carbon stocks and fluxes

Carbon stocks and fluxes are all within the range of reported values for temperate broadleaves (Pregitzer and Euskirchen, 2004; Luyssaert et al., 2007). The 7% difference in standing aboveground wood between "unmanaged" and "managed" cases (Figure 6b) is smaller than existing estimates of 25%-50% for moderate to high thinning regimes (Lanier, 1994; Vetter et al., 2005). The simulated thinning regime is indeed quite extensive, with a target *rdi* of 0.75. Two other explanatory factors, the uncertainty of the self-thinning parameters and the absence of thinning-related mortality, are further discussed in the context of the sensitivity analysis below.

The flux dynamics throughout the rotation also compares well with previous studies. As in Thornton, et al. (2002), CWD decomposition drives HR, and therefore determines how quickly the stand turns into a carbon sink after a clear cut. Both the amplitude of the source and the time of recovery are within the ranges of existing modelling studies, respectively of -500 to -1 000 gC m^{-2} yr^{-1} and 10-20 years (van Oene et al., 2000; Thornton et al., 2002; Turner et al., 2005). This is also consistent with the empirical range of 700 to 1 300 gC m^{-2} yr^{-1} for the HR of temperate forests aged between 0 and 10 (Pregitzer and Euskirchen, 2004).

As found by Lloyd and Farquhar (1996), an important part of the vegetation sink is due to the lag between NPP and litterfall. The role of management however is not negligible. In the "unmanaged scenario" (ORCH-FM_u), the cumulated NEP over a rotation of 150 years – 13 500

505 gC m^{-2} – makes up only 60% of the cumulated NEP – 22 500 gC m^{-2} – in the "managed scenario"
506 (ORCH-FM_m). As much as 40% of the sink of the "managed" scenario can therefore be
507 attributed to management. This ability of ORHCIDEE-FM to simulate a positive NEP – i.e. a net
508 sink – through forest growth is an important improvement for the null average of the standard
509 steady-state simulation. While ORCHIDEE has long been able to simulate climate-related inter-
510 annual variability and long-term trends in NEP, the absence of a management-driven sink has
511 been singled out as a capital weakness of the model (Ciais et al., 2008; Luyssaert et al., 2010).
512 While the results from ORCHIDEE-FM thus confirm the recent empirical findings of positive NEP
513 in old forests (Field and Kaduk, 2004; Ciais et al., 2008; Luyssaert et al., 2008) with about 150 gC
514 m^{-2} yr^{-1} at 150 years in the ORCH-FM_m simulation, this result has to be interpreted with caution.
515 The narrowing of the gap between NPP and HR is mainly due to the parameterized age-related
516 decline in NPP. This age-related decline of 9% at 150 years is found to be on the lower end of
517 the empirical range of 0-76% (Gower et al., 1996), and much lower than the modelled value of
518 72% (Magnani et al., 2000). Yet, the decline of 50% in aboveground wood increment that
519 follows from it is consistent with yield tables (JRC, 2009), IFN data (IFN, 2008), and other
520 modelling studies (Zaehle et al., 2006). This suggests that our empirical approach to age-related
521 decline of stand NPP leads to a higher than observed wood increment decline to NPP decline
522 ratio. A higher age-related value of $decl_{factor}$ – more consistent with estimates of age-decline in
523 NPP but less consistent with estimates of age-related decline in wood increment – would give a
524 lower, if not negative, value of NEP for old forests. This contradiction calls for an improvement
525 in the allocation framework of ORCHIDEE. Attempting such an improvement will be most

meaningful when a future inclusion of the nitrogen cycle allows for more variation in the allocation to leaves.

Note that the simulated effect of a thinning is a decrease in NPP, which means that the effect of GPP decrease overcomes the effect of harvest on autotrophic respiration. Finally, the increase in HR and decrease in NPP creates a temporary but strong 150 gC m^{-2} yr^{-1} decrease of NEP following thinnings. Empirical evidence regarding the effect of a partial and temporary defoliation – such as a defoliation due to thinning – on NEP is mixed: Vesala et al. (2005) and Granier et al. (2008) find no significant effect while Allard et al. (2008) attributes a 25% decrease in NEP to an insect-induced defoliation. In particular, a compensating increase in understory GPP, which has been shown to occur in a Finnish forest (Vesala et al., 2005), would be missed by ORCHIDEE-FM which does not represent the understory. For these reasons, the simulated effect of thinnings on NEP has to be interpreted with caution.

22.2 Parameterisation and sensitivity analysis

22.2.1 Initial distribution of trees

As these parameters ($dens_{init}$, $circ\_init_{min}$, p_{max}) are probably the least well known, the small sensitivity of model results to them is an important result. Nevertheless, the high uncertainty associated with these parameters means they could vary by more than 50%. A narrower initial distribution for example – with a p_{max} increased five-fold, leading to an initial maximum circumference decreased by 27% – leads to a narrower distribution throughout the whole rotation (see appendix 25.2.2). Unfortunately, measurements in densely stocked young stands

546 are challenging and the literature on stand characteristics during the very first years after
547 harvest is scarce. The only reference we have is for initial biomass. At 2.5 tC ha^{-1} – or about
548 1.5% of before-cut biomass – the value simulated by ORCHIDEE-FM is close to the 1% of before-
549 cut biomass used by Vetter et al. (2005).

550 22.2.2 Accuracy of the thinning parameters

551 Parameters dealing with the relative density index (σ, rdi_{lim}, rdi_{target}, and $selfth_{curve}$) are shown to
552 be among the most sensitive in the FMM. These parameters, though better known than those
553 governing initial distribution, still carry a relatively high uncertainty: rdi_{lim} and rdi_{target} are quite
554 specific to the modelling strategy of the FMM, and therefore not often reported in the
555 literature. σ and $selfth_{curve}$ have a wider theoretical interest (Jack and Long, 1996; Dhôte, 1999),
556 but reviews of estimates for a wide range of species and climate conditions are still lacking.
557 Such studies could greatly improve the accuracy of the FMM.
558 In the meantime, in order to ensure that our default values are not erroneous, we analysed the
559 thinning pattern that follows from these parameters. The cumulated thinned volume to total
560 volume produced before clear cut ratio, for example, is close to 0.55. This thinning pattern is on
561 the higher end of the 0.3-0.5 range of previous European-scale modelling studies (Nabuurs et
562 al., 2000; Nabuurs et al., 2002), but in the middle of the 0.5-0.6 range of relevant French yield
563 tables at the end of the rotation (Vannière, 1984). This comparison shows that the thinning
564 pattern simulated by the FMM is realistic, though the average European practice may yield
565 lower thinned volumes. Taken together with the small difference in standing biomass between
566 the “managed” and “unmanaged” simulations (see 22.1), this observation calls for a re-

evaluation of the self-thinning curve towards denser stands if the self-thinning scenario is to be used at European scale.

22.2.3 Allometries

The literature is abundant on the topic (Zianis and Mencuccini, 2004), but also points to species-specific variations (Vallet et al., 2006). Adding height as an explanatory variable for biomass has also been shown to improve the fit significantly (Joosten et al., 2004; Vallet et al., 2006). Refining this allometry, for example by the assimilation of remotely sensed height and/or biomass would therefore be a promising avenue of improvement for ORCHIDEE-FM.

22.2.4 Correlated effects and threshold effects

More than sensitivity alone, Figure 9 points to couples of parameters that have similar effects on model results, and to parameters exhibiting a non-linear effect:

- Branch ratio and branch turnover have the same impact on most variables trough branch mortality. They only differ by their impact on the exported volume to total volume produced ratio which is only affected by branch ratio.
- Similarly, modulating the self-thinning equation ($selfth_{curve}$) or the rdi_{target} have the same qualitative impact on most variables as they both determine the acceptable tree density to quadratic mean diameter ratio.
- When the circumference threshold σ above which basal area increase takes off (see Figure 3 and equation 2) is increased by 50%, it becomes higher than most tree circumferences. As most trees are below the threshold, they all receive a more or less

equal share of the wood increment, which results in a narrow circumference distribution. This explains the higher minimum circumference and lower maximum circumference observed on Figure 9.

22.3 Modelling strategy

22.3.1 Model coupling: averaged runs vs full-coupling

In the Ecosystem Demography model, Moorcroft *et al.* (2001) do not opt of a full coupling between the GVM and a small-scale gap model. They derive the predictions of their gap model along the two most important variables, namely tree size and age since last disturbance, and apply the simplified derived function to their GVM. This approach makes sense when the small-scale model is stochastic in order to obtain the deterministic solutions expected from large-scale GVMs while keeping computing time manageable. In this study however, we adopted a full-coupling strategy between ORCHIDEE and the FMM yet on annual time scale, more akin to Friend et al. (1997). This strategy makes it easier to analyse the effect of management at large scales: it is possible to cut off some processes and/or amplify others, and directly keep track of the result at large scales. As the FMM is strictly deterministic, a single run per location and per age class is sufficient, helping to minimize additional computing time (8 seconds – 0.5% – more than the standard version of ORCHIDEE per rotation and per site).

22.3.2 Model limitations and non-simulated processes

The FMM ignores several minor stand-scale processes involved in stand dynamics over the long term and after anthropogenic thinning. While being negligible over a standard rotation, the

absence of natural regeneration in the FMM would lead to unrealistic results over the long term if no clear cut is prescribed: left to itself, the FMM would end up with a single enormous tree after a millennium. This problem also precludes the FMM from simulating uneven-aged types of management such as the selective logging widely practiced in primary tropical forests. In temperate regions however, this management type remains uncommon (Jaccaud, 2007). Regarding anthropogenic thinning, only two processes are simulated by the FMM: the biomass transfers linked to the felling of trees and the recovery of the maximum leaf area index as the branches of surviving trees fill the gaps. Other processes have been shown to occur after an anthropogenic thinning: some mortality in damaged but unharvested trees, a possible boost in productivity, a possible change in assimilate allocation and some adjustment in biomass-circumference allometries (Mitchell, 2000; Petritsch et al., 2007; Nabuurs et al., 2008). As the quantification of these processes is still very uncertain, they are ignored in the FMM.

23 Conclusion

This study describes the structure and typical results of the new ORCHIDEE-FM model. This model calculates stand and management characteristics such as stand density, tree size distribution, tree growth, the timing and intensity of thinnings, wood removals from the stand and litter generated after thinning. The general pattern simulated for a grid cell in north-eastern France was shown to be consistent with existing studies on carbon fluxes and stocks, both in absolute values and dynamics. In particular, they confirm the possibility that forests could still act as carbon sinks after a hundred years. Anthropogenic thinning leads to biomass export from the stand and decreases the litter substrate for respiration, thus explaining 40% of

the sink throughout the rotation. A thorough model-data comparison is the object of a follow-up article, at three different scales: tree, stand and regional (Bellassen et al., Part 2, this issue). The sensitivity analysis reveals 4 major leads for improvement. Two lie in the model structure itself: an in-depth study of the impact of the initial tree circumference distribution and a review of the allocation framework of ORCHIDEE to strike a better balance between age-related decline in NPP and age-related decline in wood increment. The other two require the assimilation of local information: both the self-thinning curve and the circumference-biomass allometry have been shown to be very sensitive parameters in the FMM. The most promising way of increasing their accuracy would to fit them locally based on the dominant species, tree height and/or soil fertility. We suspect that the use of remote sensing data could bridge the gap between the large scale of GVMs and the smaller scale at which this type of information is usually collected.

Overall, our investigation supports the notion that including forest management in DGVMs will reveal a more realistic picture of biosphere-atmosphere interactions, future carbon sequestration and vulnerability of land carbon pools to climate change than focusing solely on natural forests at equilibrium.

24 Acknowledgements

We want to acknowledge the contribution of Antoine Colin (IFN), Daniel Rittié (INRA-LERFoB), and Maurizio Teobaldelli (JRC) without whom the work on the datasets they manage would have been both impossible and meaningless. We also want to thank Eric Dufrêne (CNRS-ESE) and Soenke Zaehle (MPI) for their useful suggestions on the model structure, and Sebastiaan

649 Luyssaert (LSCE) and Laurent Saint-André (CIRAD) for their valuable comments on the
650 manuscript.
651 This work was funded by the French Ministry for Research. It benefited from data generated by
652 the CarboEurope-IP project. This study contributes to the French ANR AUTREMENT project
653 (ANR-06-PADD-002).

654 25 Appendixes

655 *25.1 Age-related decline in NPP*

656 The age-related decline factor of photosynthesis efficiency decreases linearly with age, down to
657 a maximum age-related decline factor of $decl_{max}$ (cf. Eq. 1, main text).

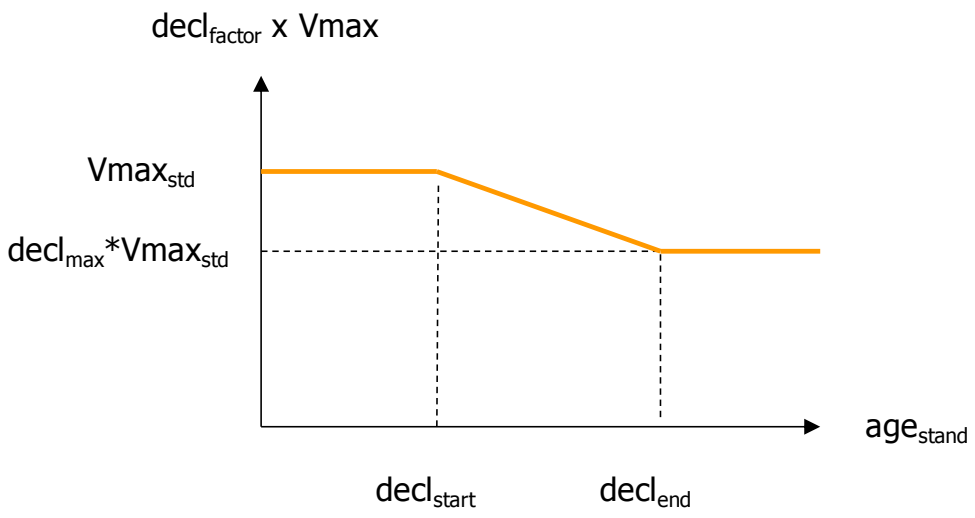

658

659 Figure A 1 illustrates this process.

25.2 Initial distribution

25.2.1 Algorithm

The intial tree circumference distribution follows a truncated exponential law of parameter λ resulting from the following algorithm:

- A minimum initial circumference, $circ\_init_{min}$, is selected.
- The exponential distribution is truncated so that unlikely values do not appear. $circ\_init_{max}$, the maximum initial circumference, is selected so that:

$$P(X < circ\_init_{max}) = 1 - p_{max} \text{ with pmax set at } \frac{100}{n_{maxtrees}} \quad \textbf{(A1)}$$

- The $[circ\_init_{min}, circ\_init_{max}]$ interval is divided into 20 intervals.
- The number of trees n_i in each interval [a,b] is proportional to $P(a \le X < b)$:

$$n_i = \left(\exp(-\lambda b) - \exp(-\lambda a)\right) \times n_{maxtrees} \quad \textbf{(A2)}$$

- These numbers are rounded to the closest integer, and the number of trees of each intervals are adjusted so that:

$$\sum_i n_i = n_{maxtrees} \quad \textbf{(A3)}$$

- Tree circumferences are then equally distributed in each interval:

$$\forall j \in n_i \; circ_j = a + b \times \frac{j}{n_i} \quad \textbf{(A4)}$$

The resulting distribution is illustrated in

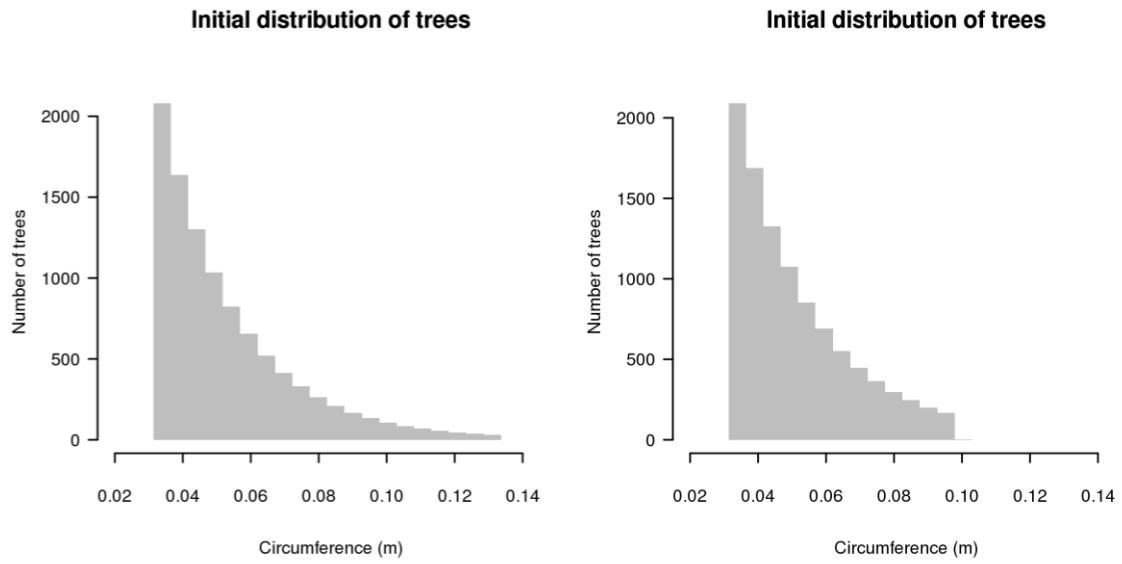

a. $p_{max} = 100/n_{maxtreees}$ b. $p_{max} = 500/n_{maxtreees}$

677

678 Figure A 2.

679 **25.2.2 Impact of a more condensed initial distribution**

680 If p_{max} is increased 5-fold, $circ\_init_{max}$ is decreased by 27%, leading to a more condensed

681 distribution (see

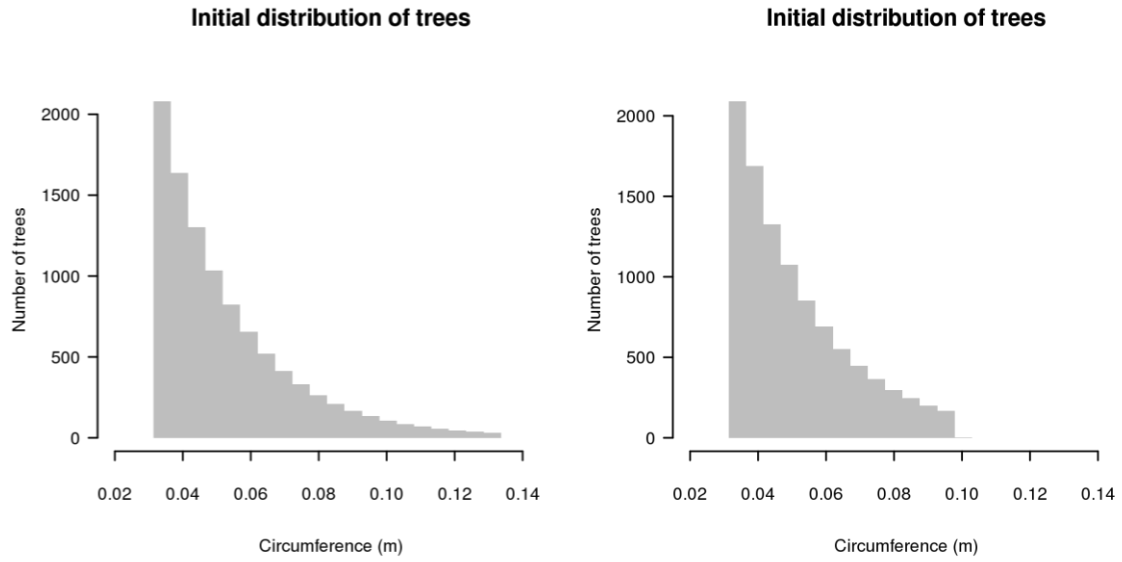

a. $p_{max} = 100/n_{maxtreees}$ b. $p_{max} = 500/n_{maxtreees}$

682

683 Figure A 2b).

684 *25.3 Calibration of the height-circumference allometry*

685 To calibrate the height-circumference allometry, we restricted the national inventory data set
686 (IFN, 2008) along the following stand criteria: high forests, dedicated to wood production, with
687 a known tree density, a closed canopy, and a basal area greater than 10 m^2 ha^{-1}. Broadleaf and
688 needleleaf stands were fitted separately. The Gauss-Newton non-linear algorithm was then
689 used to fit the allometry.

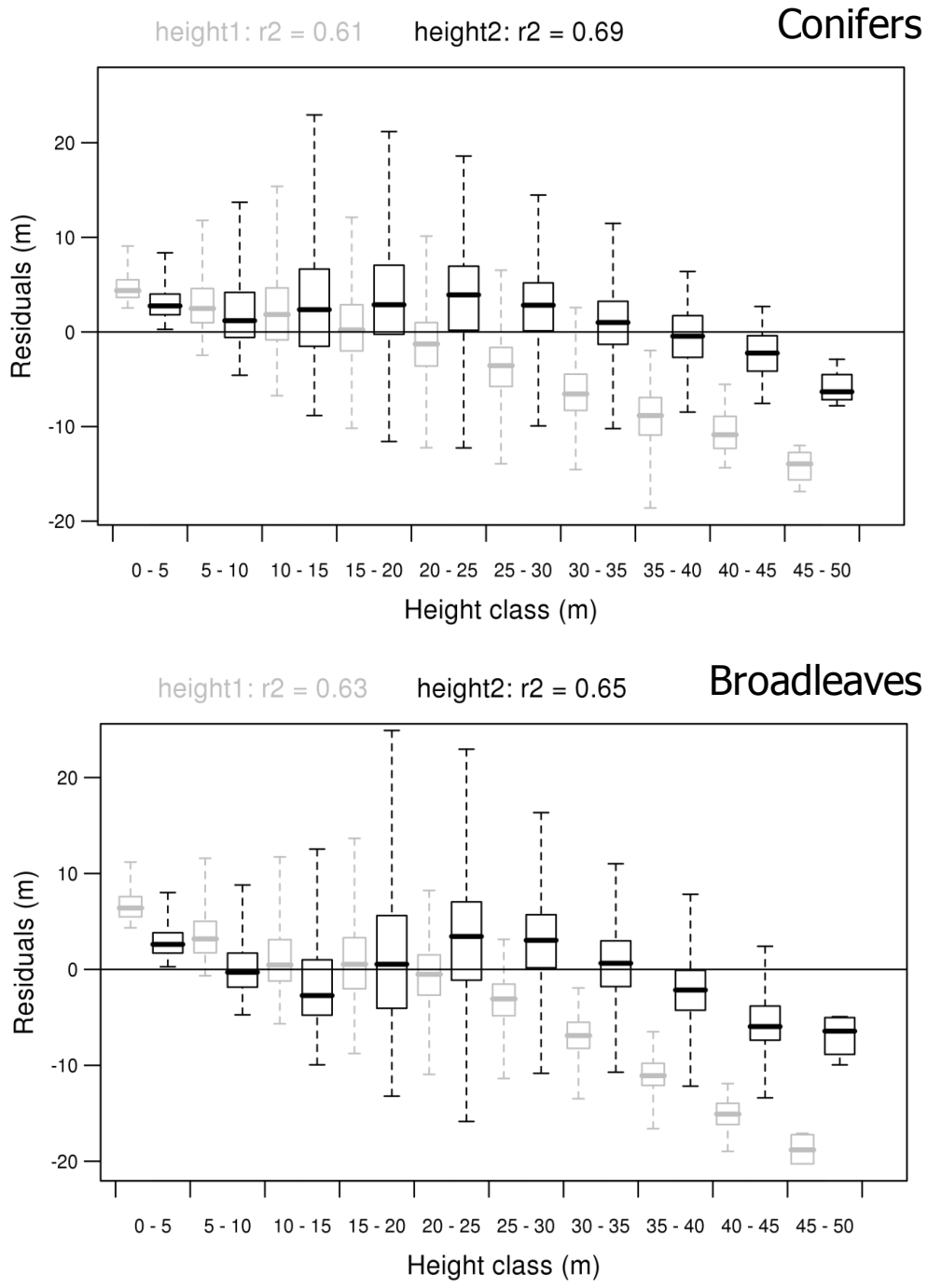

690

691 Figure A 3 shows that the residuals of the allometric model used in the FMM, “height model 2”,

692 are less biased for large trees than those of a simpler model, “height model 1” (Eq. (A5)).

$$\text{height}_i = 1.3 + \alpha \times \left(1 - \exp\left(-\delta \times \text{circ}_i\right)^{\varphi}\right) \quad \textbf{(A5)}$$

where $height_i$ and $circ_i$ are respectively the height and circumference of tree i in m, and α, δ, and φ are parameters.

25.4 Thinning strategy (th_{strat})

In order to determine which trees are felled during a thinning event (be it natural or anthropogenic), a probability of death τ_i is attributed to each tree Eq. (A4). The value of the parameter th_{strat} sets the thinning strategy: if $th_{strat} > 0$, a "thinning from below" strategy is simulated, with smaller trees preferentially thinned to obtain larger logs in the future. If $th_{strat} < 0$, a "thinning from above" strategy is simulated, with larger trees preferentially thinned thus giving way to smaller trees.

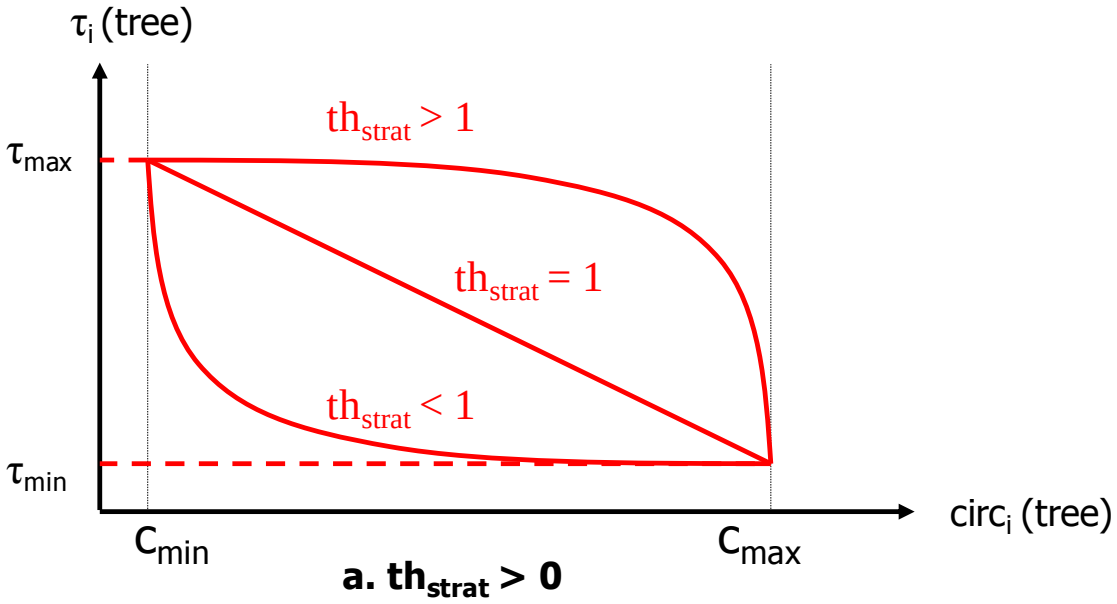

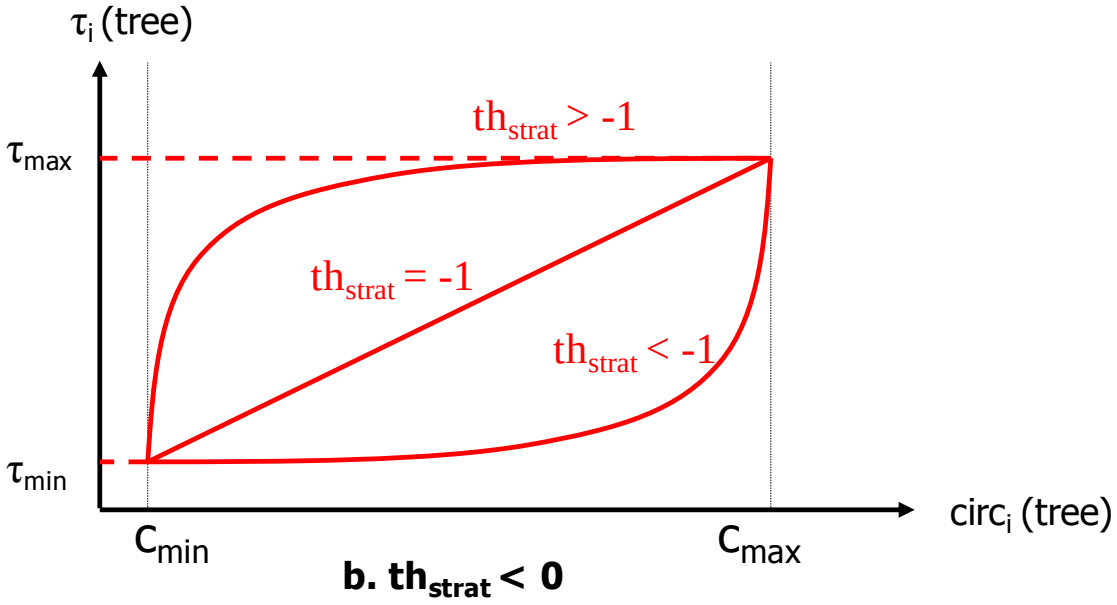

703

704 Figure A 4 illustrates this algorithm.

25.5 Initial conditions ("spinup")

As computing time is increased when ORCHIDEE is coupled to the FMM, the "spinup" is performed in two steps. First, ORCHIDEE without the FMM is repeatedly run for the 1997 climate and a CO_2 concentration of 380 ppm until all ecosystem carbon and water pools reach their steady state equilibrium. Using this first steady state as initial conditions, ORCHIDEE is then run with the FMM for seventeen rotations (that is 2550 years), using the same climatic conditions. After seventeen rotations, the soil carbon pool reaches a new cyclic steady state (see

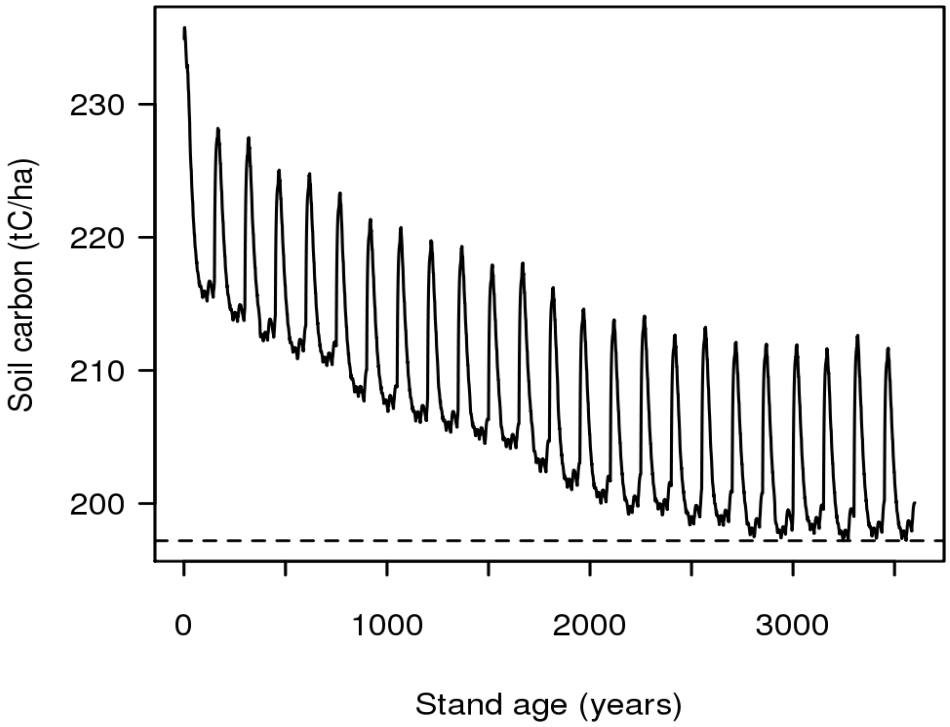

713

714 Figure A 5). The conditions of the stand before the last clearcut are used as initial conditions for

715 all subsequent simulations.

716 *25.6 Evolution of tree circumference distribution over a forest rotation*

717 The simulated evolution of tree circumference distribution over a forest rotation is illustrated

718 by

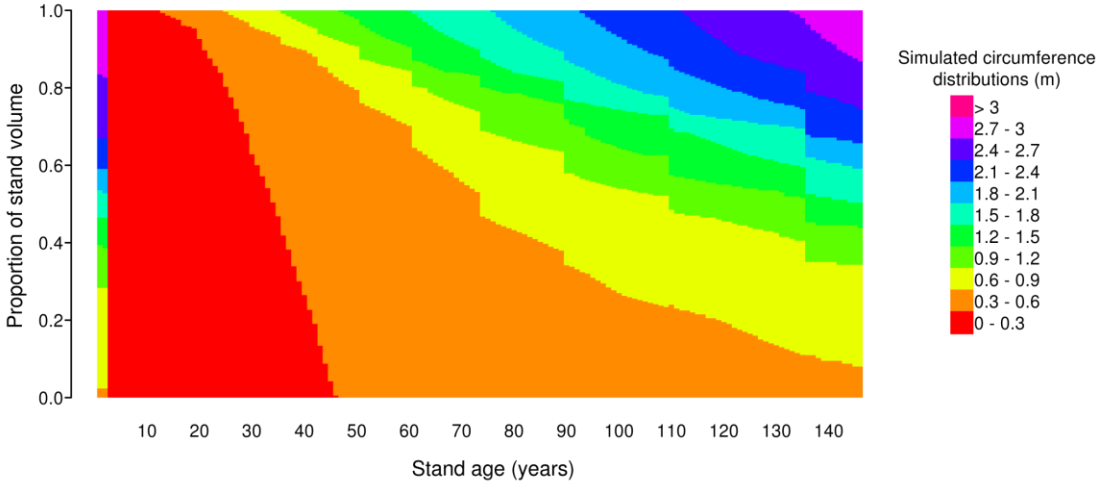

719

720 Figure A 6.

721 # 26 References

722 Allard, V., Ourcival, J.M., Rambal, S., Joffre, R. and Rocheteau, A., 2008. Seasonal and annual
723 variation of carbon exchange in an evergreen Mediterranean forest in southern France. Global
724 Change Biology, 14:714-725.
725 Asael, S., 1999. Typologie des peuplements forestiers du massif vosgiens, C.R.P.F. Lorraine-
726 Alsace, Nancy, 54 p.
727 Bellassen, V., Le Maire, G., Guin, O., Dhote, J.F., Viovy, N. and Ciais, P., 2010. Modeling
728 forest management within a global vegetation model – Part 2: model validation from tree to
729 continental scale. Ecological Modelling.
730 Botta, A., Viovy, N., Ciais, P., Friedlingstein, P. and Monfray, P., 2000. A global prognostic
731 scheme of leaf onset using satellite data. Global Change Biology, 6:709-725.
732 Bottcher, H., Freibauer, A., Obersteiner, M. and Schulze, E.D., 2008. Uncertainty analysis of
733 climate change mitigation options in the forestry sector using a generic carbon budget model.
734 Ecological Modelling, 213:45-62.
735 Bouriaud, O., 2003. Analyse fonctionnelle de la productivité du hêtre : influence des conditions
736 du milieu, de la structure du peuplement et du couvert, effets de l'éclaircie, Ecole Nationale du
737 Génie Rural des Eaux et des Forêts, Nancy, 320 p
738 Bugmann, H., 2001. A review of forest gap models. Climatic Change, pp. 259-305.
739 Carvalhais, N., Reichstein, M., Ciais, P., Collatz, G.J., Mahecha, M., Montagnani, L., Papale, D.,
740 Rambal, S. and Seixas, J., 2010. Identification of Vegetation and Soil Carbon Pools out of
741 Equilibrium in a Process Model via Eddy Covariance and Biometric Constraints. Global Change
742 Biology, in press.

743 Cazin, A., Vallet, P. and Dhote, J.F., 2003. Propositions LERFoB pour CARBOFOR - Atelier
744 modélisation.
745 Ciais, P., Schelhaas, M.J., Zaehle, S., Piao, S.L., Cescatti, A., Liski, J., Luyssaert, S., Le-Maire,
746 G., Schulze, E.D., Bouriaud, O., Freibauer, A., Valentini, R. and Nabuurs, G.J., 2008. Carbon
747 accumulation in European forests. Nature Geoscience, 1:425-429.
748 Deleuze, C., Pain, O., Dhote, J.F. and Herve, J.C., 2004. A flexible radial increment model for
749 individual trees in pure even-aged stands. Annals of Forest Science, 61:327-335.
750 Desai, A.R., Moorcroft, P.R., Bolstad, P.V. and Davis, K.J., 2007. Regional carbon fluxes from
751 an observationally constrained dynamic ecosystem model: Impacts of disturbance, CO2
752 fertilization, and heterogeneous land cover. Journal of Geophysical Research-Biogeosciences,
753 112.
754 Dhôte, J.-F. and Hervé, J.-C., 2000. Changements de productivité dans quatre forêts de chênes
755 sessiles depuis 1930 : une approche au niveau du peuplement. Ann. For. Sci., 57:651-680.
756 Dhôte, J.F., 1999. Compétition entre classes sociales chez le chêne sessile et le hêtre. Revue
757 Forestière Française:309-325.
758 Dhôte, J.F. and Le Moguédec, G., 2003. Présentation du modèle Fagacées, INRA, 31 p p.
759 Ducoudre, N.I., Laval, K. and Perrier, A., 1993. SECHIBA, a new set of parameterizations of the
760 hydrologic exchanges at the land atmosphere interface within the LMD atmospheric general-
761 circulation model. Journal of Climate, 6:248-273.
762 European Commission, 2005. Biomass Action Plan. Communication from the CommissionNo.
763 COM(2005) 628, Brussels, 47 p.
764 Field, C.B. and Kaduk, J., 2004. The carbon balance of an old-growth forest: Building across
765 approaches. Ecosystems, 7:525-533.
766 Franklin, O., Aoki, K. and Seidl, R., 2009. A generic model of thinning and stand density effects
767 on forest growth, mortality and net increment. Annals of Forest Science, 66:815p811-815p811.
768 Friend, A.D., Stevens, A.K., Knox, R.G. and Cannell, M.G.R., 1997. A process-based, terrestrial
769 biosphere model of ecosystem dynamics (Hybrid v3.0). Ecological Modelling, 95:249-287.
770 Gower, S.T., McMurtrie, R.E. and Murty, D., 1996. Aboveground net primary production
771 decline with stand age: Potential causes. Trends in Ecology & Evolution, 11:378-382.
772 Granier, A., Breda, N., Longdoz, B., Gross, P. and Ngao, J., 2008. Ten years of fluxes and stand
773 growth in a young beech forest at Hesse, North-eastern France. Annals of Forest Science,
774 65:704p701-704p711.
775 Grote, R. and Erhard, M., 1999. Simulation of tree and stand development under different
776 environmental conditions with a physiologically based model. Forest Ecology and Management,
777 120:59-76.
778 Hoffmann, F., 1995. FAGUS, a model for growth and development of beech. Ecological
779 Modelling, 83:327-348.
780 Hurtt, G.C., Dubayah, R., Drake, J., Moorcroft, P.R., Pacala, S.W., Blair, J.B. and Fearon, M.G.,
781 2004. Beyond potential vegetation: combining lidar data and a height-structured model for
782 carbon studies. Ecological Applications, 14:873-883.
783 IFN, 2006. Observer la forêt française : mission première de l'IFN. L'IF:12.
784 IFN, 2008. Raw inventory data, www.ifn.fr.
785 Jaccaud, T., 2007. La forêt en France. L'Ecologiste, 23:38-39.
786 Jack, S.B. and Long, J.N., 1996. Linkages between silviculture and ecology: An analysis of
787 density management diagrams. Forest Ecology and Management, 86:205-220.

788 Joosten, R., Schumacher, J., Wirth, C. and Schulte, A., 2004. Evaluating tree carbon predictions
789 for beech (Fagus sylvatica L.) in western Germany. Forest Ecology and Management, 189:87-96.
790 JRC, 2009. European Forest Yield Table's database,
791 http://afoludata.jrc.ec.europa.eu/DS_Free/abc_intro.cfm.
792 Jung, M., Le Maire, G., Zaehle, S., Luyssaert, S., Vetter, M., Churkina, G., Ciais, P., Viovy, N.
793 and Reichstein, M., 2007. Assessing the ability of three land ecosystem models to simulate gross
794 carbon uptake of forests from boreal to Mediterranean climate in Europe. Biogeosciences, 4:647-
795 656.
796 Kalnay, E., Kanamitsu, M., Kistler, R., Collins, W., Deaven, D., Gandin, L., Iredell, M., Saha,
797 S., White, G., Woollen, J., Zhu, Y., Chelliah, M., Ebisuzaki, W., Higgins, W., Janowiak, J., Mo,
798 K.C., Ropelewski, C., Wang, J., Leetmaa, A., Reynolds, R., Jenne, R. and Joseph, D., 1996. The
799 NCEP/NCAR 40-year reanalysis project. Bulletin of the American Meteorological Society,
800 77:437-471.
801 Krinner, G., Viovy, N., de Noblet-Ducoudre, N., Ogee, J., Polcher, J., Friedlingstein, P., Ciais,
802 P., Sitch, S. and Prentice, I.C., 2005. A dynamic global vegetation model for studies of the
803 coupled atmosphere-biosphere system. Global Biogeochemical Cycles, 19:44.
804 Lanier, L., 1994. Précis de sylviculture. Ecole Nationale du Génie Rural, des Eaux et des Forêts
805 (ENGREF), Nancy, 477 p.
806 Le Dantec, V., Dufrene, E. and Saugier, B., 2000. Interannual and spatial variation in maximum
807 leaf area index of temperate deciduous stands. Forest Ecology and Management, 134:71-81.
808 Lefsky, M.A., Turner, D.P., Guzy, M. and Cohen, W.B., 2005. Combining lidar estimates of
809 aboveground biomass and Landsat estimates of stand age for spatially extensive validation of
810 modeled forest productivity. Remote Sensing of Environment, 95:549.
811 Lindner, M., Lucht, W., Bouriaud, O., Green, T. and Janssens, I., 2004. Specific Study on Forest
812 Greenhouse Gas Budget, CarboEurope-GHG, Jena, 62 p.
813 Lischke, H., Zimmermann, N.E., Bolliger, J., Rickebusch, S. and Löffler, T.J., 2006. TreeMig: A
814 forest-landscape model for simulating spatio-temporal patterns from stand to landscape scale.
815 Ecological Modelling, 199:409.
816 Lloyd, J. and Farquhar, G.D., 1996. The CO2 dependence of photosynthesis, plant growth
817 responses to elevated atmospheric CO2 concentrations and their interaction with soil nutrient
818 status .1. General principles and forest ecosystems. Functional Ecology, 10:4-32.
819 Loustau, D., 2004. Rapport final du projet CARBOFOR, INRA, Bordeaux, 138 p.
820 Luyssaert, S., Ciais, P., Piao, S.L., Schulze, E.D., Jung, M., Zaehle, S., Schelhaas, M.J.,
821 Reichstein, M., Churkina, G., Papale, D., Abril, G., Beer, C., Grace, J., Loustau, D., Matteucci,
822 G., Magnani, F., Nabuurs, G.J., Verbeeck, H., Sulkava, M., van der Werf, G.R., Janssens, I.A.
823 and Team, C.-I.S., 2010. The European carbon balance. Part 3: forests. Global Change Biology,
824 16:1429-1450.
825 Luyssaert, S., Inglima, I., Jung, M., Richardson, A.D., Reichsteins, M., Papale, D., Piao, S.L.,
826 Schulzes, E.D., Wingate, L., Matteucci, G., Aragao, L., Aubinet, M., Beers, C., Bernhoffer, C.,
827 Black, K.G., Bonal, D., Bonnefond, J.M., Chambers, J., Ciais, P., Cook, B., Davis, K.J., Dolman,
828 A.J., Gielen, B., Goulden, M., Grace, J., Granier, A., Grelle, A., Griffis, T., Grunwald, T.,
829 Guidolotti, G., Hanson, P.J., Harding, R., Hollinger, D.Y., Hutyra, L.R., Kolar, P., Kruijt, B.,
830 Kutsch, W., Lagergren, F., Laurila, T., Law, B.E., Le Maire, G., Lindroth, A., Loustau, D.,
831 Malhi, Y., Mateus, J., Migliavacca, M., Misson, L., Montagnani, L., Moncrieff, J., Moors, E.,
832 Munger, J.W., Nikinmaa, E., Ollinger, S.V., Pita, G., Rebmann, C., Roupsard, O., Saigusa, N.,

Sanz, M.J., Seufert, G., Sierra, C., Smith, M.L., Tang, J., Valentini, R., Vesala, T. and Janssens, I.A., 2007. CO2 balance of boreal, temperate, and tropical forests derived from a global database. Global Change Biology, 13:2509-2537.
Luyssaert, S., Schulze, E.D., Borner, A., Knohl, A., Hessenmoller, D., Law, B.E., Ciais, P. and Grace, J., 2008. Old-growth forests as global carbon sinks. Nature, 455:213-215.
Magnani, F., Mencuccini, M. and Grace, J., 2000. Age-related decline in stand productivity: the role of structural acclimation under hydraulic constraints. Plant Cell and Environment, 23:251-263.
Marti, O., Braconnot, P., Dufresne, J.L., Bellier, J., Benshila, R., Bony, S., Brockmann, P., Cadule, P., Caubel, A., Codron, F., de Noblet, N., Denvil, S., Fairhead, L., Fichefet, T., Foujols, M.A., Friedlingstein, P., Goosse, H., Grandpeix, J.Y., Guilyardi, E., Hourdin, F., Idelkadi, A., Kageyama, M., Krinner, G., Levy, C., Madec, G., Mignot, J., Musat, I., Swingedouw, D. and Talandier, C., 2010. Key features of the IPSL ocean atmosphere model and its sensitivity to atmospheric resolution. Climate Dynamics, 34:1-26.
Masera, O.R., Garza-Caligaris, J.F., Kanninen, M., Karjalainen, T., Liski, J., Nabuurs, G.J., Pussinen, A., de Jong, B.H.J., Mohren, G.M.J. and Tz, 2003. Modeling carbon sequestration in afforestation, agroforestry and forest management projects: the CO2FIX V.2 approach. Ecological Modelling, 164:177-199.
Mitchell, S.J., 2000. Stem growth responses in Douglas-fir and Sitka spruce following thinning: implications for assessing wind-firmness. Forest Ecology and Management, 135:105.
Mokany, K., Raison, R.J. and Prokushkin, A.S., 2006. Critical analysis of root: shoot ratios in terrestrial biomes. Global Change Biology, 12:84-96.
Moorcroft, P.R., Hurtt, G.C. and Pacala, S.W., 2001. A method for scaling vegetation dynamics: The ecosystem demography model (ED). Ecological Monographs, 71:557-585.
Murty, D. and McMurtrie, R.E., 2000. The decline of forest productivity as stands age: a model-based method for analysing causes for the decline. Ecological Modelling, 134:185.
Nabuurs, G.J., Pussinen, A., Karjalainen, T., Erhard, M. and Kramer, K., 2002. Stemwood volume increment changes in European forests due to climate change - a simulation study with the EFISCEN model. Global Change Biology, 8:304-316.
Nabuurs, G.J., Schelhaas, M.J. and Pussinen, A., 2000. Validation of the European Forest Information Scenario Model (EFISCEN) and a projection of Finnish forests. pp. 167-179.
Nabuurs, G.J., van Putten, B., Knippers, T.S. and Mohren, G.M.J., 2008. Comparison of uncertainties in carbon sequestration estimates for a tropical and a temperate forest. Forest Ecology and Management, 256:237-245.
Nagy, M.T., Janssens, I.A., Yuste, J.C., Carrara, A. and Ceulemans, R., 2006. Footprint adjusted net ecosystem CO2 exchange and carbon balance components of a temperate forest. Agricultural and Forest Meteorology, 139:344-360.
Newton, R.F. and Amponsah, I.G., 2007. Comparative evaluation of five height-diameter models developed for black spruce and jack pine stand-types in terms of goodness-of-fit, lack-of-fit and predictive ability. Forest Ecology and Management, 247:149-166.
Olsson, B.A., Staaf, H., Lundkvist, H., Bengtsson, J. and Rosen, K., 1996. Carbon and nitrogen in coniferous forest soils after clear-felling and harvests of different intensity. Forest Ecology and Management, 82:19-32.
Ovington, J.D. and Madgwick, H.A.I., 1957. Afforestation and soil reaction. Journal of Soil Science, 8:141-149.

878 Pacala, S.W., Canham, C.D., Saponara, J., Silander, J.A., Kobe, R.K. and Ribbens, E., 1996.
879 Forest models defined by field measurements: Estimation, error analysis and dynamics.
880 Ecological Monographs, 66:1-43.
881 Parton, W.J., Stewart, J.W.B. and Cole, C.V., 1988. Dynamics of C, N, P and S in grassland soils
882 - A model. Biogeochemistry, 5:109-131.
883 Petritsch, R., Hasenauer, H. and Pietsch, S.A., 2007. Incorporating forest growth response to
884 thinning within biome-BGC. Forest Ecology and Management, 242:324-336.
885 Pregitzer, K.S. and Euskirchen, E.S., 2004. Carbon cycling and storage in world forests: biome
886 patterns related to forest age. Global Change Biology, 10:2052-2077.
887 Pretzsch, H., Biber, P. and Durský, J., 2002. The single tree-based stand simulator SILVA:
888 construction, application and evaluation. Forest Ecology and Management, 162:3.
889 Reineke, L.H., 1933. Perfecting a stand-density index for even-aged forests. Journal of
890 Agricultural Research, 46:627-638.
891 Ryan, M.G., Phillips, N. and Bond, B.J., 2006. The hydraulic limitation hypothesis revisited.
892 Plant Cell and Environment, 29:367-381.
893 Saint-Andre, A., Laclau, J.-P., Deleporte, P., Gava, J.L., Goncalves, J.L.M., Mendham, D.,
894 Nzila, J.D., Smith, C., du Toit, B., Xu, D.P., Sankaran, K.V., Marien, J.N., Nouvellon, Y.,
895 Bouillet, J.P. and Ranger, J., 2008. Slash and Litter Management Effects on Eucalyptus
896 Productivity: a Synthesis Using a Growth and Yield Modelling Approach. In: E.K. Sadanandan
897 Nambiar (Editor), Site management and productivity in tropical plantation forests : Proceedings
898 of Workshops in Piracicaba (Brazil) 22-26 November 2004 and Bogor (Indonesia) 6-9
899 November 2006. CIFOR, Jakarta, pp. 173-189.
900 Sato, H., Itoh, A. and Kohyama, T., 2007. SEIB-DGVM: A new dynamic global vegetation
901 model using a spatially explicit individual-based approach. Ecological Modelling, 200:279-307.
902 Schaefer, K., Collatz, G.J., Tans, P., Denning, A.S., Baker, I., Berry, J., Prihodko, L., Suits, N.
903 and Philpott, A., 2008. Combined Simple Biosphere/Carnegie-Ames-Stanford Approach
904 terrestrial carbon cycle model. Journal of Geophysical Research-Biogeosciences, 113:13.
905 Schelhaas, M.J., van Esch, T.A., Groen, B.H.J., Kanninen, M., Liski, J., Masera, O.R., Mohren,
906 G.M.J., Nabuurs, G.J., Palosuo, T., Pedroni, L., Vallejo, A. and Vilén, T., 2004. CO2FIX V 3.1 -
907 A modelling framework for quantifying carbon sequestration in forest ecosystems Alterra-
908 rapport No. 1068, Alterra, Wageningen, 122 p.
909 Shevliakova, E., Pacala, S.W., Malyshev, S., Hurtt, G.C., Milly, P.C.D., Caspersen, J.P.,
910 Sentman, L.T., Fisk, J.P., Wirth, C. and Crevoisier, C., 2009. Carbon cycling under 300 years of
911 land use change: Importance of the secondary vegetation sink. Global Biogeochemical Cycles,
912 23.
913 Sitch, S., Huntingford, C., Gedney, N., Levy, P.E., Lomas, M., Piao, S.L., Betts, R., Ciais, P.,
914 Cox, P., Friedlingstein, P., Jones, C.D., Prentice, I.C. and Woodward, F.I., 2008. Evaluation of
915 the terrestrial carbon cycle, future plant geography and climate-carbon cycle feedbacks using
916 five Dynamic Global Vegetation Models (DGVMs). Global Change Biology, 14:2015-2039.
917 Thornton, P.E., Law, B.E., Gholz, H.L., Clark, K.L., Falge, E., Ellsworth, D.S., Golstein, A.H.,
918 Monson, R.K., Hollinger, D., Falk, M., Chen, J. and Sparks, J.P., 2002. Modeling and measuring
919 the effects of disturbance history and climate on carbon and water budgets in evergreen
920 needleleaf forests. Agricultural and Forest Meteorology, 113:185-222.
921 Turner, D.P., Ritts, W.D., Cohen, W.B., Maeirsperger, T.K., Gower, S.T., Kirschbaum, A.A.,
922 Running, S.W., Zhao, M.S., Wofsy, S.C., Dunn, A.L., Law, B.E., Campbell, J.L., Oechel, W.C.,

923 Kwon, H.J., Meyers, T.P., Small, E.E., Kurc, S.A. and Gamon, J.A., 2005. Site-level evaluation
924 of satellite-based global terrestrial gross primary production and net primary production
925 monitoring. Global Change Biology, 11:666-684.
926 Vacchiano, G., Motta, R., Long, J.N. and Shaw, J.D., 2008. A density management diagram for
927 Scots pine (Pinus sylvestris L.): A tool for assessing the forest's protective effect. Forest Ecology
928 and Management, 255:2542-2554.
929 Valentine, H.T. and Mäkelä, A., 2005. Bridging process-based and empirical approaches to
930 modeling tree growth. Tree Physiology, 25:769-779.
931 Vallet, P., Dhote, J.F., Le Moguedec, G., Ravart, M. and Pignard, G., 2006. Development of total
932 aboveground volume equations for seven important forest tree species in France. Forest Ecology
933 and Management, 229:98-110.
934 van Oene, H., Berendse, F., Persson, T., Harrison, A.F., Schulze, E.D., Andersen, B.R., Bauer,
935 G.A., Dambrine, E., Hogberg, P., Matteucci, G. and Paces, T., 2000. Model Analysis of Carbon
936 and Nitrogen Cycling in Picea and Fagus Forests. In: E.D. Schulze (Editor), Carbon and
937 Nitrogen Cycling in European Forest Ecosystems. Springer-Verlag, Heidelberg, p. 500.
938 Vannière, B., 1984. Tables de production pour les forêts françaises. Ecole Nationale du Génie
939 Rural, des Eaux et des Forêts, Nancy, 160 p.
940 Vesala, T., Suni, T., Rannik, U., Keronen, P., Markkanen, T., Sevanto, S., Gronholm, T.,
941 Smolander, S., Kulmala, M., Ilvesniemi, H., Ojansuu, R., Uotila, A., Levula, J., Mäkelä, A.,
942 Pumpanen, J., Kolari, P., Kulmala, L., Altimir, N., Berninger, F., Nikinmaa, E. and Hari, P.,
943 2005. Effect of thinning on surface fluxes in a boreal forest. Global Biogeochemical Cycles, 19.
944 Vetter, M., Churkina, G., Jung, M., Reichstein, M., Zaehle, S., Bondeau, A., Chen, Y., Ciais, P.,
945 Feser, F., Freibauer, A., Geyer, R., Jones, C., Papale, D., Tenhunen, J., Tomelleri, E., Trusilova,
946 K., Viovy, N. and Heimann, M., 2008. Analyzing the causes and spatial pattern of the European
947 2003 carbon flux anomaly using seven models. Biogeosciences, 5:561-583.
948 Vetter, M., Wirth, C., Bottcher, H., Churkina, G., Schulze, E.D., Wutzler, T. and Weber, G.,
949 2005. Partitioning direct and indirect human-induced effects on carbon sequestration of managed
950 coniferous forests using model simulations and forest inventories. Global Change Biology,
951 11:810-827.
952 Vieira, I.C.G., de Almeida, A.S., Davidson, E.A., Stone, T.A., de Carvalho, C.J.R. and Guerrero,
953 J.B., 2003. Classifying successional forests using Landsat spectral properties and ecological
954 characteristics in eastern Amazonia. Remote Sensing of Environment, 87:470-481.
955 Viovy, N., Calvet, J.C., Ciais, P., Dolman, A.J., Gusev, Y., El Mayaar, M., Moors, E., Nasanova,
956 O., Pitman, A., Polcher, J., Rivalland, V., Shmakin, A. and Verseghy, D., 2010. The PILPS-
957 CARBON model evaluation experiment: a test bed for simulating water, energy and carbon
958 exchange over a forest canopy. unpublished data.
959 Yang, Y. and Titus, S.J., 2002. Maximum size-density relationship for constraining individual
960 tree mortality functions. Forest Ecology and Management, 168:259-273.
961 Zaehle, S., Sitch, S., Prentice, I.C., Liski, J., Cramer, W., Erhard, M., Hickler, T. and Smith, B.,
962 2006. The importance of age-related decline in forest NPP for modeling regional carbon
963 balances. Ecological Applications, 16:1555-1574.
964 Zianis, D. and Mencuccini, M., 2004. On simplifying allometric analyses of forest biomass.
965 Forest Ecology and Management, 187:311-332.
966
967

Tables

Table 1. Parameters names and their default values

Name	Description	Value for broadleaves	Value for coniferous	Unit	Sources	Equation	Section
$decl_{max}$	Maximum age-related decline in photosynthesis efficiency	0.95	0.90	no unit	Teobaldelli et al. 2008, Gower et al., 1996	1	2.2.2
$decl_{start}$	Age at wich age-related decline of NPP starts	50	same	year	Gower et al., 1996, Magnani et al., 2000	1	2.2.2
$branch_{ratio}$	Ratio of branches over total aboveground biomass	0.38	0.25	no unit	Loustau 2004, Le Maire 2005	na	2.2.2
$branch_{turn}$	Proportion of branches dying each day	2.5	same	$\%.year^{-1}$	Masera 2003, van Oene 2000	na	2.2.2
$branch_{sap/heart}$	Sapwood/Heartwood ratio in branches	0.5	same	no unit	Hoffmann 1995	na	2.2.2
τ_{cwd}	Maximum turnover rate of coarse woody debris	0.75	same	$year^{-1}$	Olsson 1996, Schelaas 2004, Nagy 2006	na	2.2.2
$alloc_{min}$	Minimum aboveground/belowground sapwood allocation ratio	0.60	same	no unit	Mokany 2004, Nagy 2006	3	2.2.2
$alloc_{max}$	Maximum aboveground/belowground sapwood allocation ratio	0.80	same	no unit	Mokany 2004, Nagy 2006	3	2.2.2
$demi_{alloc}$	Half-life of aboveground/belowground sapwood allocation ratio increase	5.00	same	year	Mokany 2004, Nagy 2006	3	2.2.2
$n_{maxtrees}$	Initial stand density	10 000	same	$ind.ha^{-1}$	Dhôte 2003, van Oene 2000	na	2.3.2
Dg_{init}	Initial quadratic mean diameter	0.01	same	m	Dhôte 2003	4	2.3.2
m	Smoothing parameter for tree growth equation (growth=f(circumference))	1.05	same	no unit	Deleuze 2003	5	2.3.2
$pipe_{density}$	Wood density	0.3	0.2	$tC.m^{-3}$	Hoffmann 1995, Friend 1997, FCBA 2009	na	2.3.2
a_{σ}	Slope of the linear regression $ln(\sigma)=f(ln(dens))$	-0.35	same	$ln(m).ln(ind.ha)^{-1}$	Fitted on data from Dhôte 2000	6	2.3.2
b_{σ}	Intercept of the linear regression $ln(\sigma)=f(ln(dens))$	1.88	same	ln(m)	Fitted on data from Dhôte 2000	6	2.3.2
a_{bc}	Coefficient of biomass-circumference allometry	$7.03*b_{bc}^{-4.76}$	same	kgDM	Zianis 2004	7	2.3.2
b_{bc}	Coefficient of biomass-circumference allometry	2.44	2.30	$ln(kgDM).ln(m)^{-1}$	Fitted on data from IFN 2008	7	2.3.2
α_{st}	Coefficient of selth-thinning equation	min(171 582-145 248)	198 336	$ind.ha^{-1}$	Dhôte 2003, Vacchiato 2008	8	2.3.3
β_{st}	Coefficient of selth-thinning equation	min(1.7-1.57)	1.60	$ln(ind.ha^{-1}).ln(m)^{-1}$	Dhôte 2003, Vacchiato 2008	8	2.3.3
α	Coefficient of circumference-height allometry	19.42	9.30	na	Fitted on data from IFN 2008	10	2.3.3
χ	Coefficient of circumference-height allometry	0.11	0.35	na	Fitted on data from IFN 2008	10	2.3.3
δ	Coefficient of circumference-height allometry	0.13	0.13	na	Fitted on data from IFN 2008	10	2.3.3
φ	Coefficient of circumference-height allometry	0.75	0.69	na	Fitted on data from IFN 2008	10	2.3.3
Φ	Coefficient of circumference-height allometry	-0.12	-0.32	na	Fitted on data from IFN 2008	10	2.3.3
rdi_{target}	Targeted value of relative density index	0.75	same	no unit	Cazin 2003	na	2.2.3
rdi_{lim}	Width of buffer within which rdi is allowed to vary between thinnings	0.05-0.1*	same	no unit	Cazin 2003	na	2.2.3
$dens_{target}$	Target density triggering a clearcut	200	100	$ind.ha^{-1}$	Lanier 1994	na	2.3.4
age_{target}	Target age triggering a clearcut	150	same	years	Lanier 1994	na	2.3.4
th_{strat}	Thinning strategy index	1	same	no unit	Dhôte 2008	12	2.3.4
τ_{min}	Minimum relative mortality rate	0.01	same	no unit	na	12	2.3.4
τ_{max}	Maximum relative mortality rate	0.05	same	no unit	na	12	2.3.4
δlai_{max}	Proportional decrease of lai_{max} after thinning	30	same	%	Le Dantec 2000, Vesala 2005	na	2.4

*0.1 when density is nmaxtrees log-linearly decreasing to 0.05 when density is denstarget

age (years)	20	40	60	80	100	120	140
density (ind/ha)	4095	1442	684	423	279	203	153
basal area (m2/ha)	18.8	24.1	26.7	29.9	31.8	33.7	35.2
average height (m)	8.0	12.2	15.6	18.4	20.7	22.5	24.0
stand volume (m3/ha)	108	187	258	328	388	441	489
exported volume / total volume ratio	0.38	0.5	0.54	0.55	0.55	0.56	0.57
thinning frequency (years)	4	8	10	16	21	27	27
average circumference (m)	0.24	0.43	0.65	0.86	1.09	1.32	1.54
minimum circumference (m)	0.18	0.29	0.36	0.43	0.49	0.54	0.58
maximum circumference (m)	0.56	1.12	1.56	1.95	2.29	2.58	2.83

971

972 Table 2. Stand characteristics at different ages in the “managed” simulation (ORCH-FM_m)
973 Thinning frequency is defined as the time between the two thinnings surrounding the
974 corresponding age. Exported volume and total volume produced both refer to total
975 wood (including branches and stem parts with diameter lower than 7 cm).

976

Parameters			Variables	
Symbol	Full name	Equation number	Symbol	Full name
p_max	Probability threshold for truncating exponential distribution	A1	*dens*	Tree density
min_circ_init	Minimum circumference in initial distribution	A1	*ba*	Stand basal area
dens_init	Initial density	na	*av_height*	Average height
lambda	λ parameter of initial exponential distribution	2	*stand_vol*	Standing volume
height_circ	Height/circumference allometry. A value greater than 1 indicated a greater height for the same circumference.	9	*vol_exp / vol_tot*	Exported volume / Total volume produce ratio
circ_bm	Circumference/biomass allometry. A value greater than 1 indicated a greater circumference for the same biomass	5	*th_int*	Time interval between two thinnings
wood_density	Wood density	na	*av_circ*	Average circumference
branch_turn	Branch turnover rate	na	*circ_min*	Minimum circumference
branch_ratio	Branch ratio	na	*circ_max*	Maximum circumference
decl_max	Maximum age-related decline in NPP	na		
tau_spread	Range betweem maximum and minimum relative mortality rate (τ_i)	na		
th_strat	Thinning strategy	10		
selfth_curve	Self-thinning equation. A value greater than 1 indicates that a higher density is tolerated for the same quadratic mean diameter.	6		
rdi_target	Targeted value of relative density index	na		
delta_rdi	Bandwidth around rdi_target	na		
sigma	Threshold of the biomass distribution equation	3		

977

978 Table 3. Full name of the parameters and variables included in the sensitivity analysis

979

Figure captions (main text)

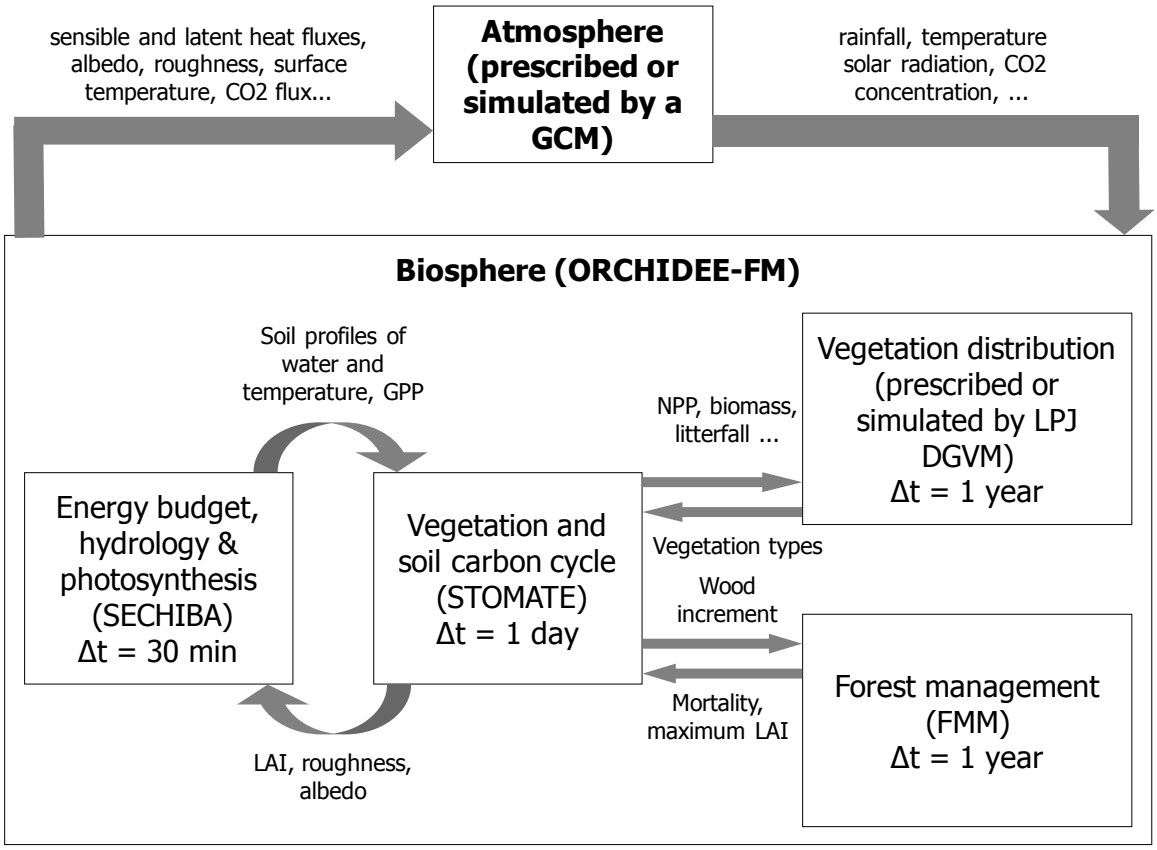

Figure 1. Structure of ORCHIDEE

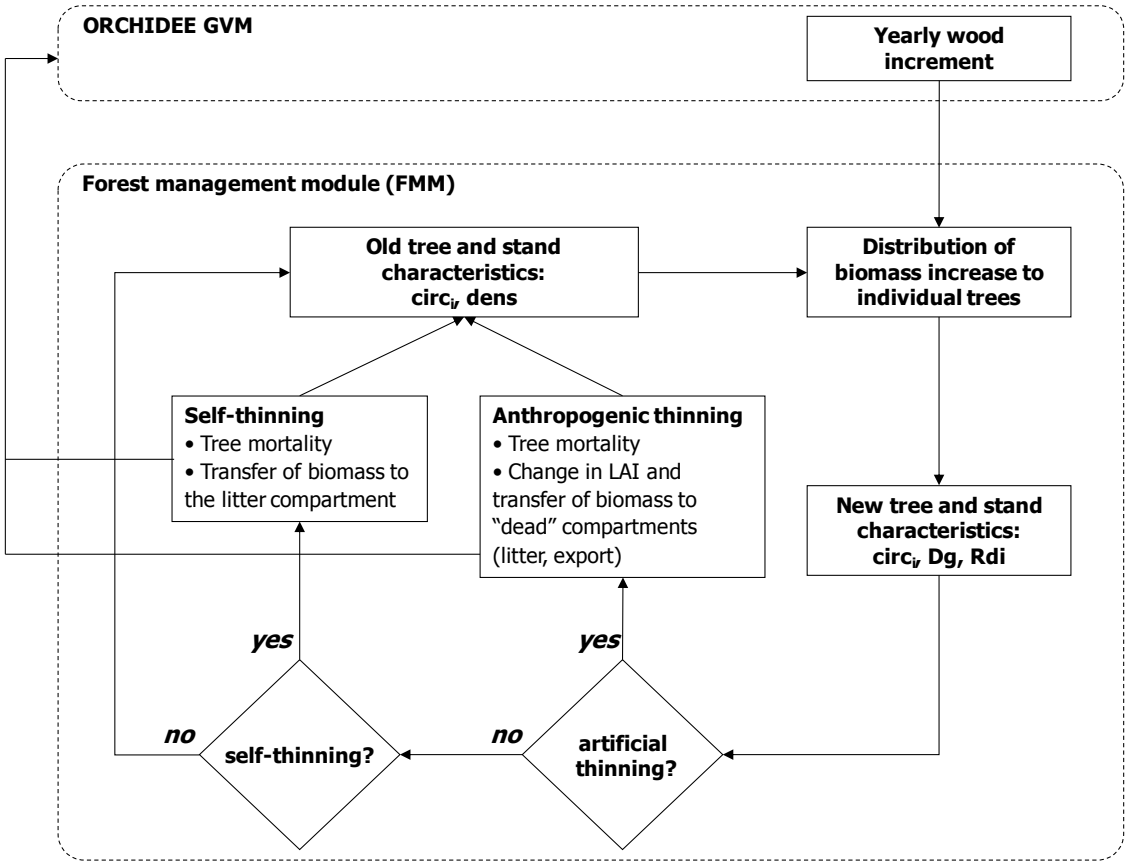

984

985 Figure 2. Conceptual diagram of the forest management module (FMM)

986 The FMM calculates mortality by explicitly simulating stand and tree characteristics: tree

987 density (*dens*), the circumference of each tree ($circ_i$), quadratic mean diameter (*Dg*),

988 relative density index (*rdi*), etc.

989

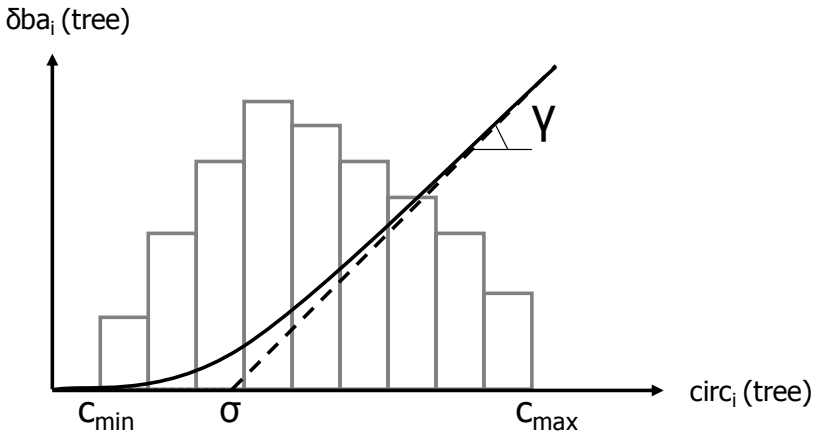

a. Increment allocation

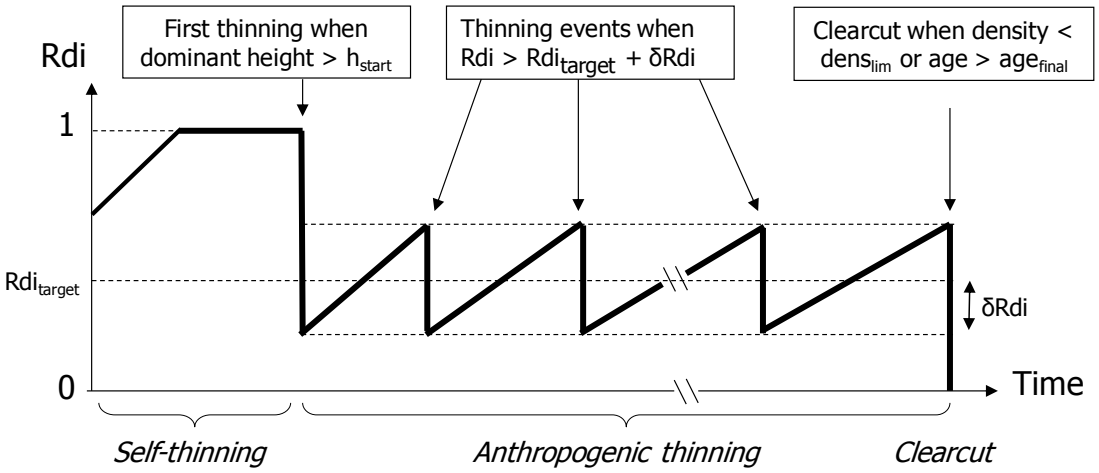

b. Thinnings

990

991 Figure 3. Increment allocation and thinnings in the FMM

992 a. Increment allocation: *σ* is the threshold circumference for growth (the basal area
993 increase of trees smaller than *σ* is close to 0) and *γ* is the slope of the
994 relationship between increase in basal area and circumference. δba_i and $circ_i$ are
995 respectively the basal area increase and circumference of tree *i*, and c_{min} and c_{max}
996 are the minimum and maximum circumferences found in the plot. Larger trees
997 get a bigger share of stand growth, and thus get a bigger increase in basal area.

b. Thinnings: the thick black line represents the evolution of *rdi* with time for a typical forest stand. In younger stands, self-thinning occurs to maintain the stand at its maximal carrying capacity (*rdi* = 1). Then, after a minimal height h_{start} is reached, human intervention maintains *rdi* around rdi_{target}. The stand is harvested when its density gets below $dens_{target}$ or its age reaches age_{final}.

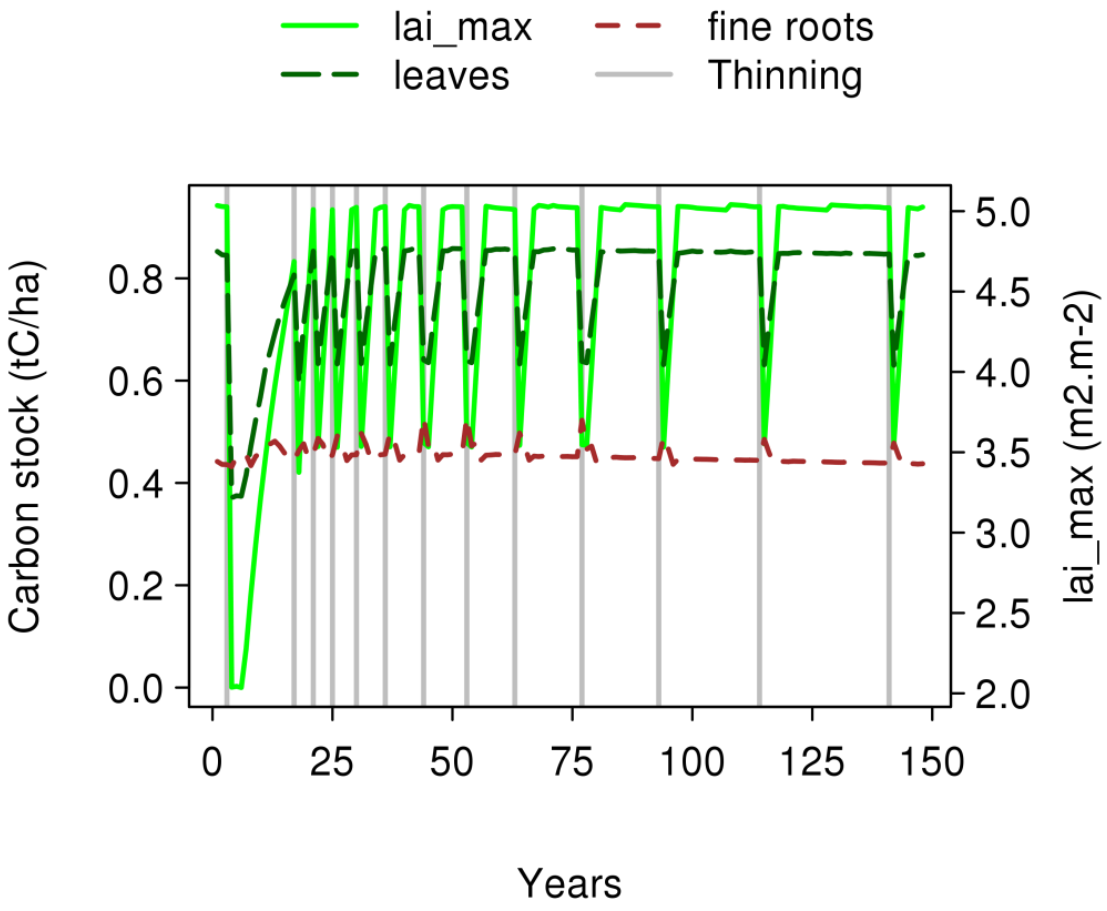

Figure 4. Lai_{max} and labile carbon stocks during a rotation period

Yearly maximum leaf area index (right axis) and yearly average carbon stocks in leaves and fine roots (left axis).

1008

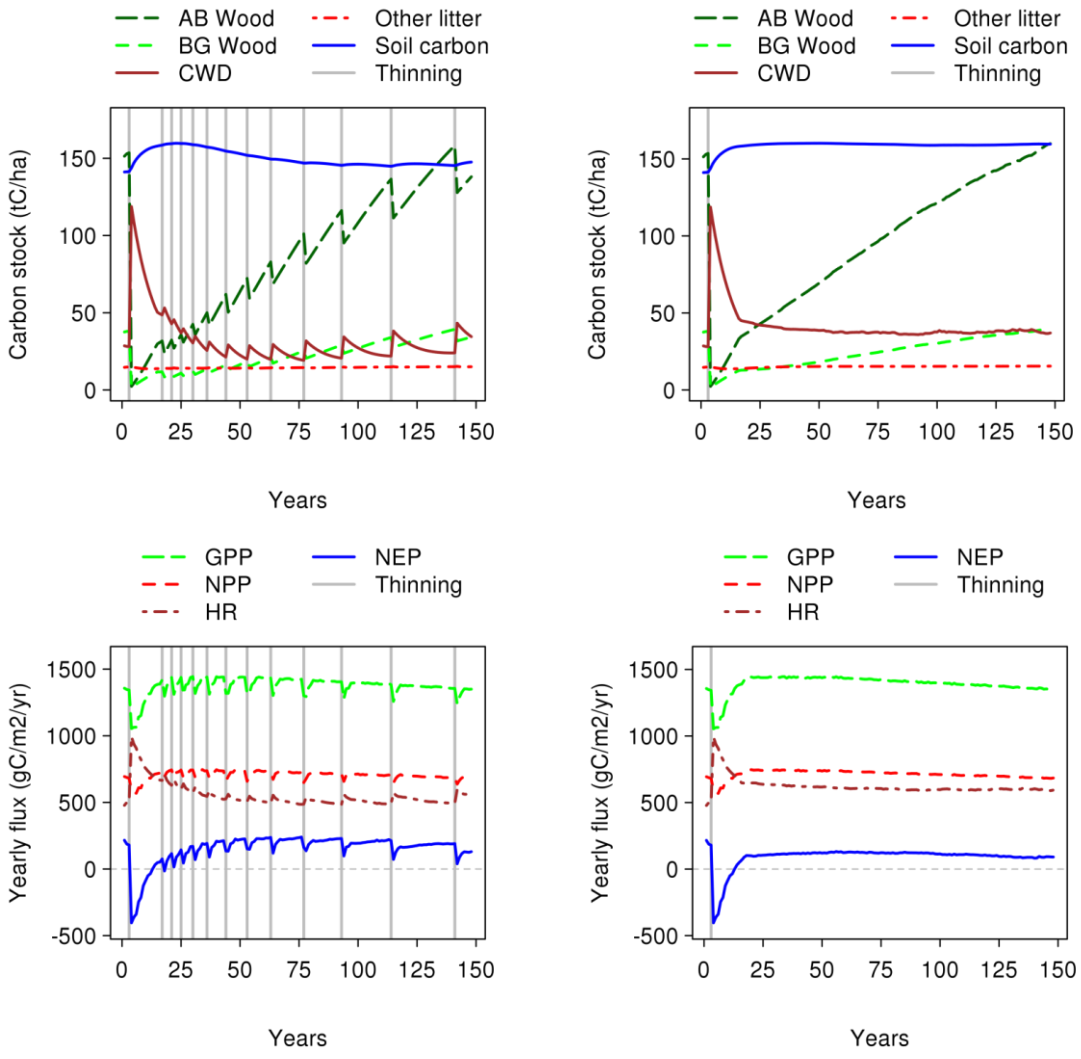

a. "Managed" case (ORCH-FM$_m$) b. "Unmanaged" case (ORCH-FM$_u$)

1009

1010 Figure 5. Simulated carbon stocks and fluxes during a rotation period

1011 Yearly average in aboveground wood (AB wood), belowground wood (BG wood), coarse

1012 woody debris (CWD), other litter (dead leaves) and soil carbon (top). Gross primary

1013 production (GPP), net primary production (NPP), heterotrophic respiration (HR), and net

1014 ecosystem productivity (bottom).

1015

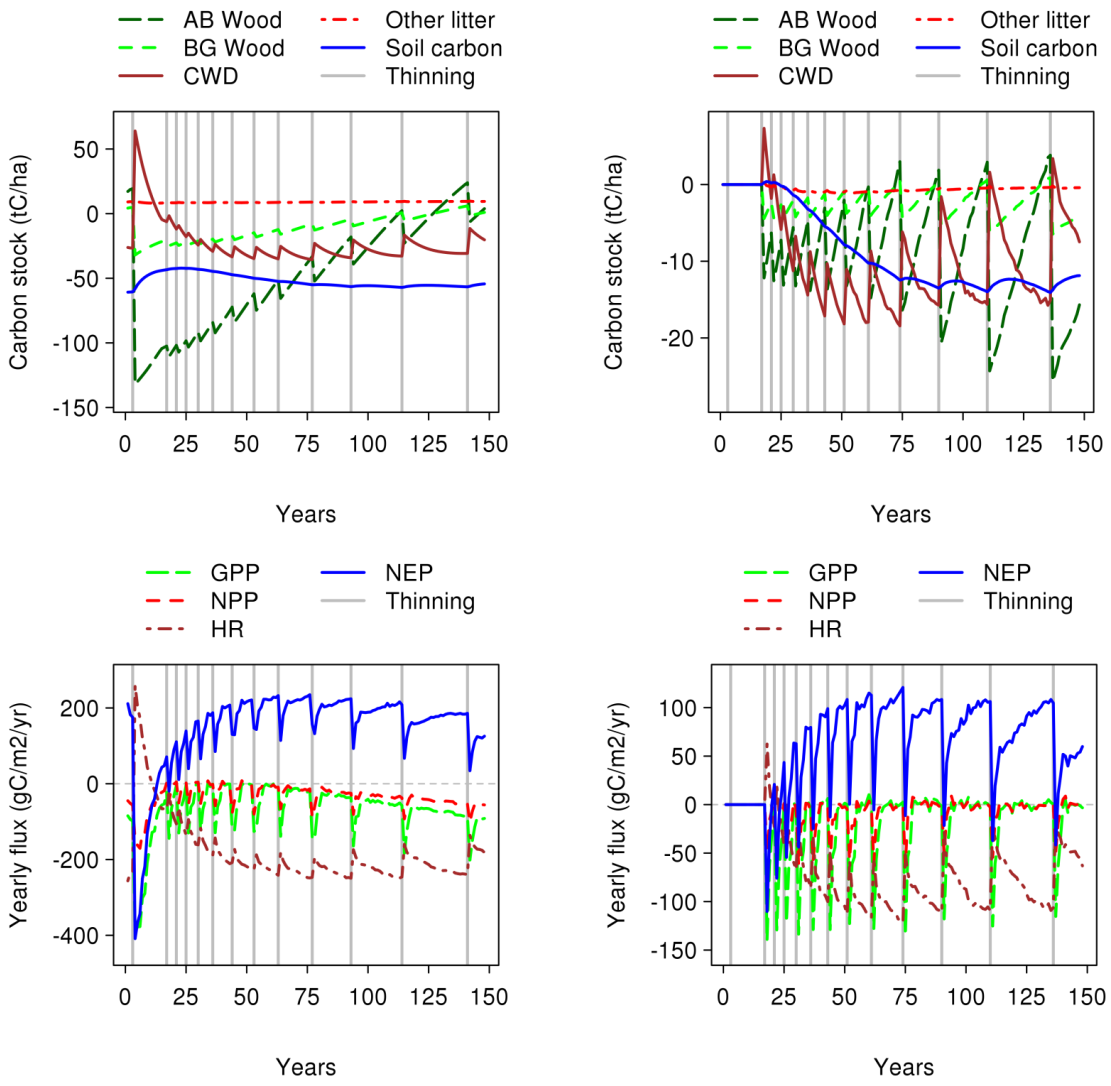

a. ORCH-FM$_m$ - ORCH-STD b. ORCH-FM$_m$ - ORCH-FM$_u$

1016

1017 Figure 6. Comparison of ORCHIDEE-FM and ORCHIDEE.

1018 The plotted curves represents the difference between the same variable simulated by

1019 (a) ORCHIDEE-FM "managed" (ORCH-FM$_m$) and ORCHIDEE (ORCH-STD) and by (b)

1020 ORCHIDEE-FM "managed" (ORCH-FM$_m$) and ORCHIDEE-FM "unmanaged" (ORCH-FM$_u$).

1021 Variables: yearly average in aboveground wood (AB wood), belowground wood (BG
1022 wood), coarse woody debris (CWD), other litter (dead leaves) and soil carbon (top).
1023 Gross primary production (GPP), net primary production (NPP), heterotrophic
1024 respiration (HR), and net ecosystem productivity (bottom).
1025

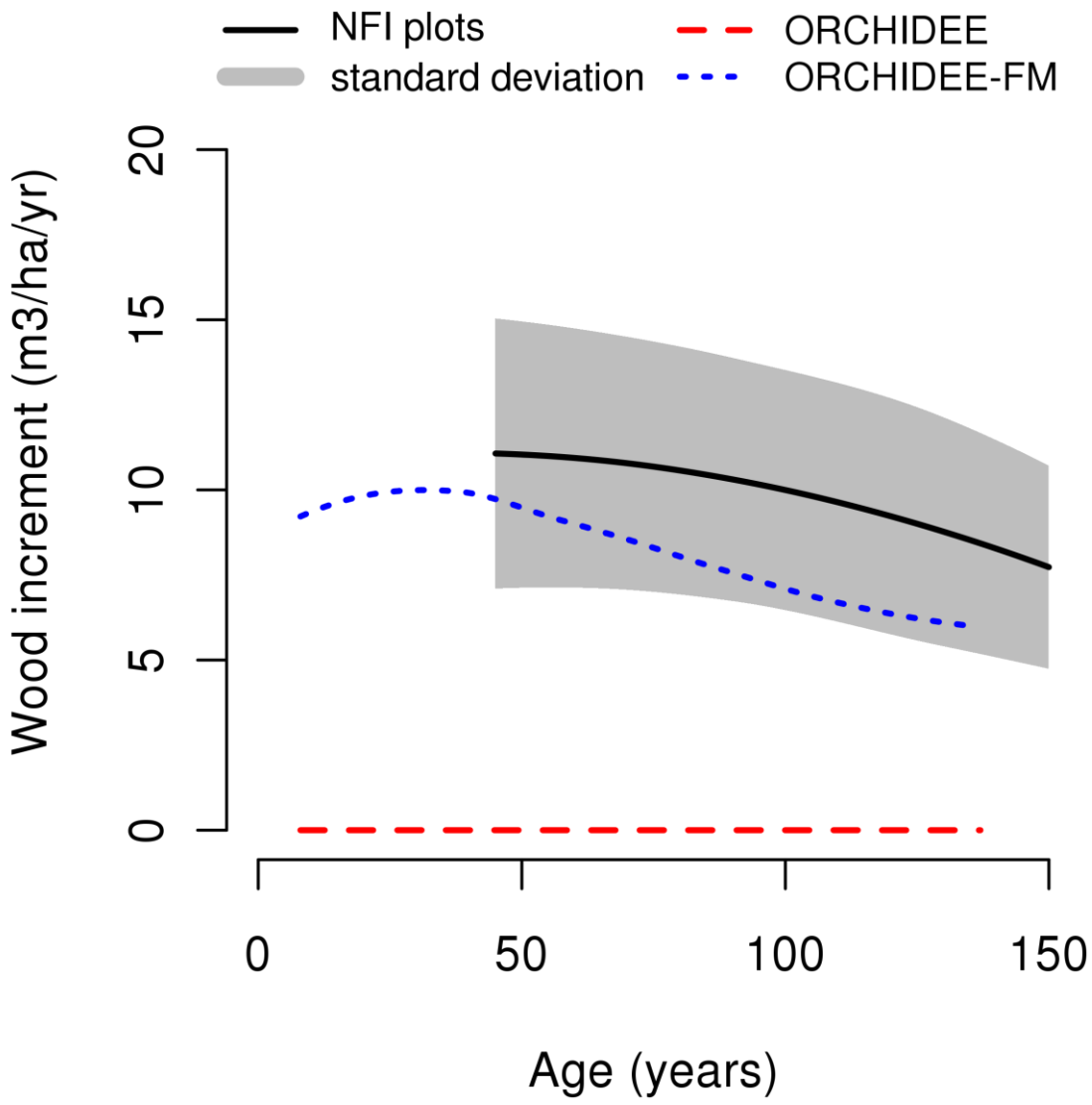

1026
1027 Figure 7. Simulated and observed wood increment close to Nancy

The black solid line and grey area respectively give the average and standard deviation of measured wood increment in National Forest Inventory (NFI) plots within a 50 km radius of our selected grid cell. Measurements are pooled per age class, and the resulting statistics per age class are smoothed using a “loess” algorithm (only age classes with 5 or more plots are retained). The large-dashed red curve and the small-dashed blue curve respectively give the wood increment in the ORCH-STD and ORCH-FM_m simulations.

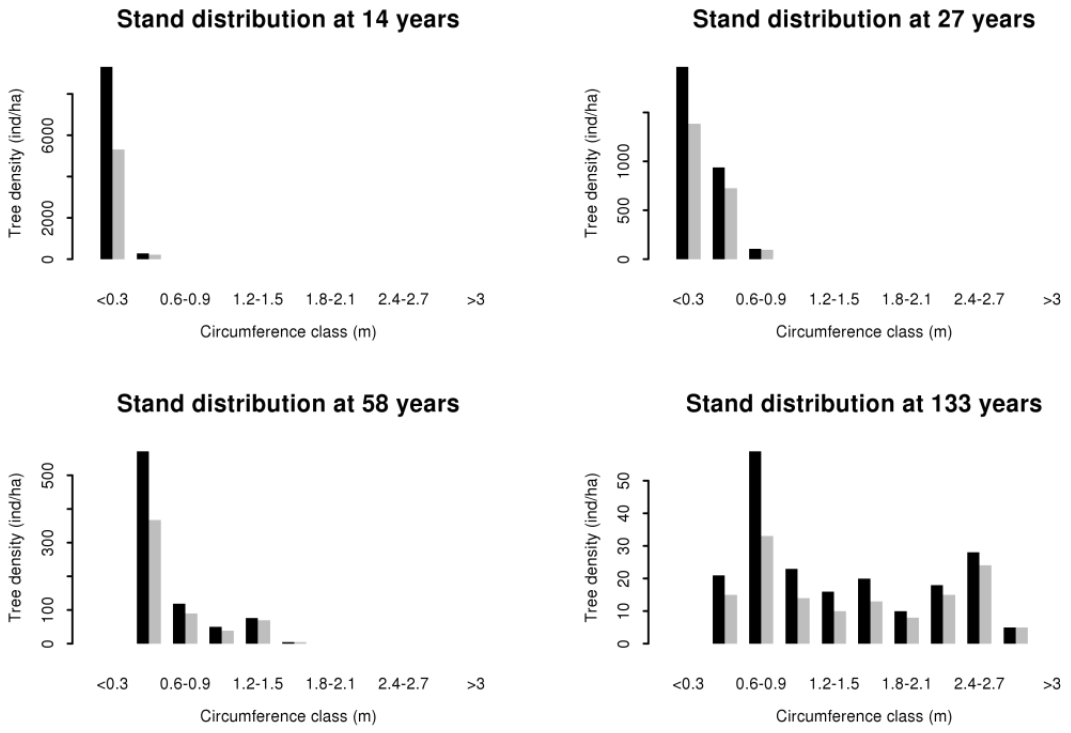

Figure 8. Tree distribution by circumference classes

Represented before (black bars) and after (grey bars) thinning for 4 selected thinning events.

1040

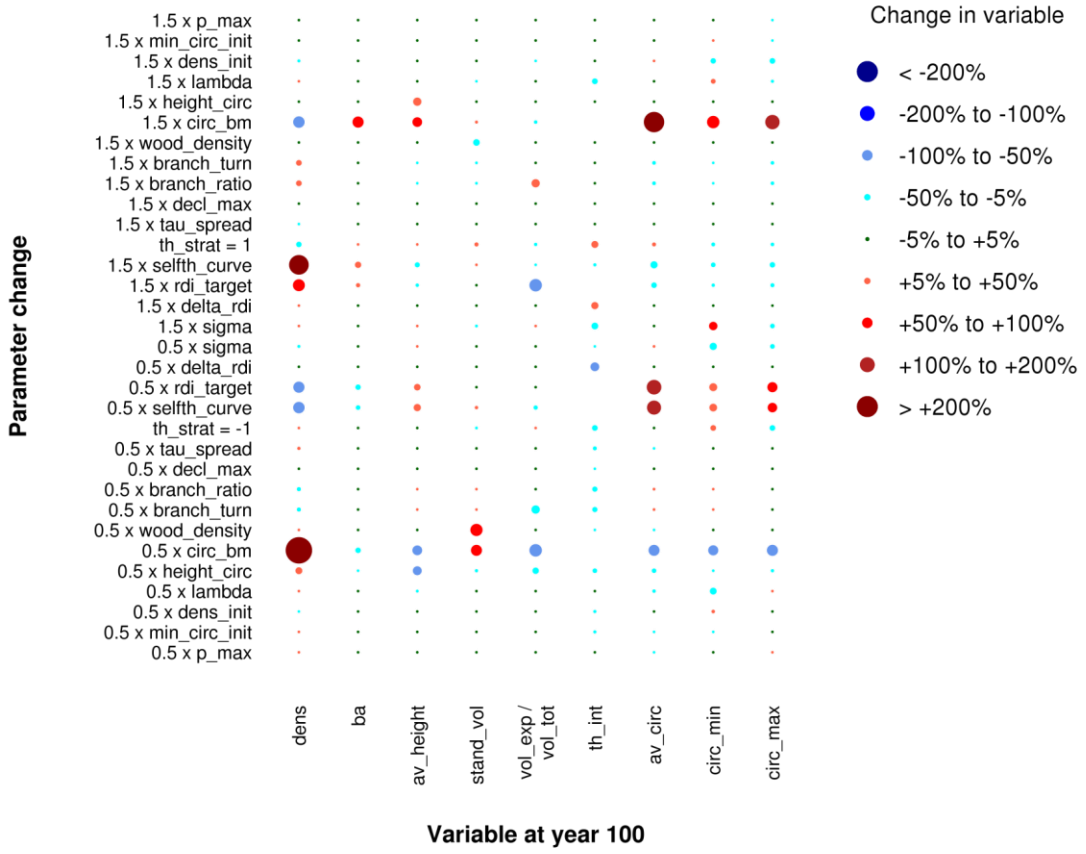

1041

1042 Figure 9. Sensitivity of 9 selected variables to changes in the values of 15 selected

1043 parameters

1044 The ordinates axis indicates by how much the default parameter value is multiplied (eg.

1045 1.5 x *lambda* indicates a model run with a *lambda* increased by 50% compared to its

1046 default value given in Table 3). The impact of this parameter change on the selected

1047 variables is represented by a full circle. The area of the circle is proportional to the

1048 absolute value of the change in the selected variable. Blue circle represent decreases

1049 and red circle represent increases. Empty values correspond to infinite changes (eg.

1050 when there is no thinning between year 100 and the end of the rotation, the thinning
1051 frequency is infinite). Table 3 lists the full names of these variables and parameters.
1052 Note that parameters are classified according to their “role” in the model (grey and
1053 white highlighting).
1054

Figure captions (appendixes)

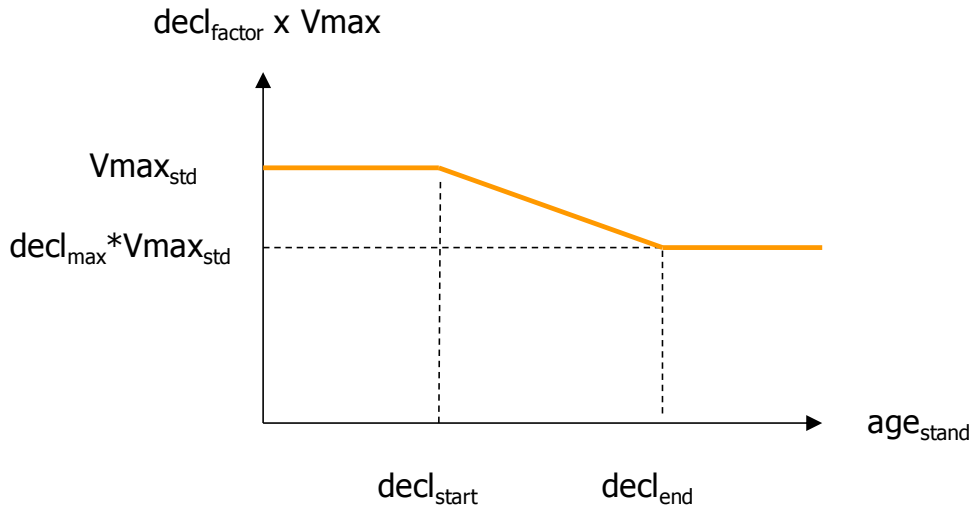

Figure A 1. Age-related decline of photosynthesis efficiency

Vmax is the photosynthesis efficiency, $Vmax_{std}$ is the standard value of *Vmax* in ORCHIDEE, *decl* is the maximum age-related decline, $decl_{start}$ and $decl_{end}$ are respectively the ages at which age-related decline starts and saturates.

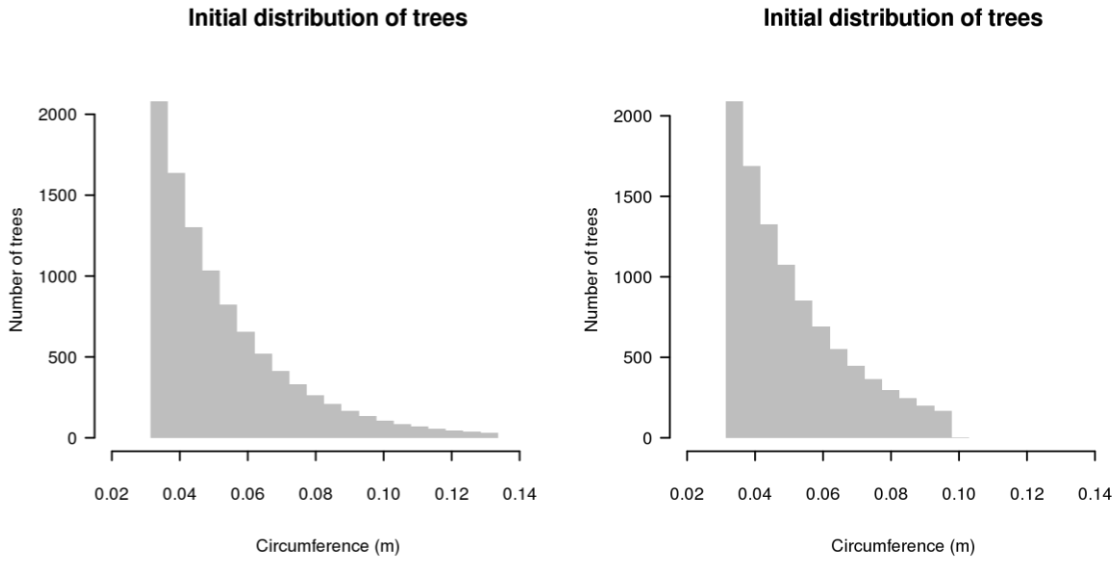

a. $p_{max} = 100/n_{maxtreees}$ b. $p_{max} = 500/n_{maxtreees}$

1062

1063 Figure A 2. Two examples of initial distributions for the same tree density ($n_{maxtrees}$ =

1064 10 000 stems per hectare): the default distribution (a) and a more condensed possibility

1065 (b). p_{max} is the probability threshold at which the distribution is truncated.

1066

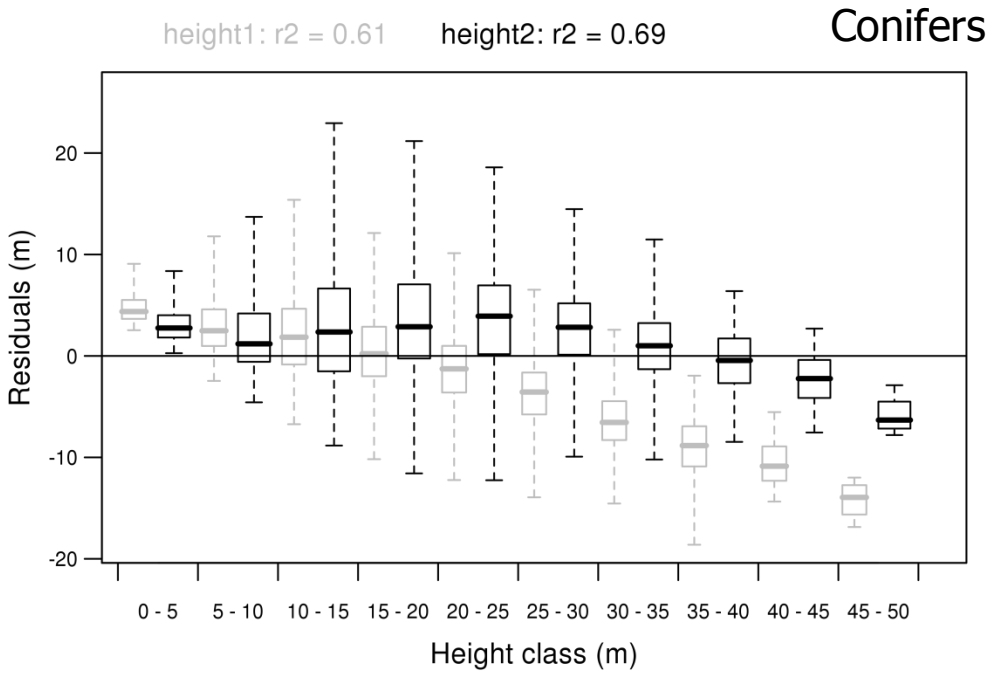

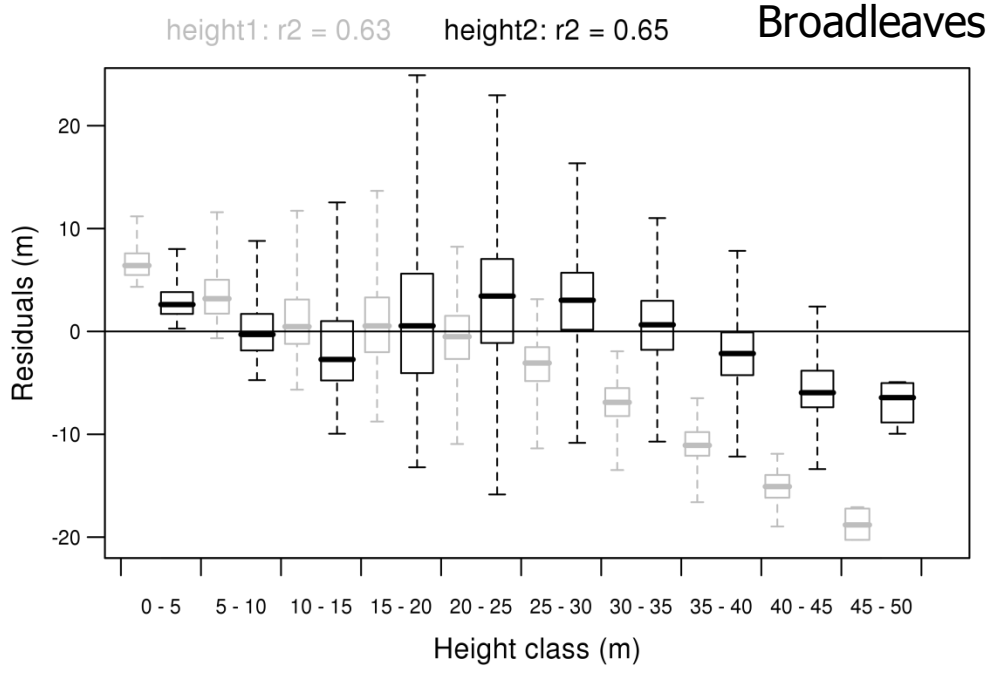

1067

1068 Figure A 3. Residuals (model – data) of the height-diameter allometry used in the FMM

1069 (height model 2) compared to a simpler allometry (height model 1) for conifers (top)

1070 and broadleaves (bottom)

1071 The whisker-plots show the median, first and third quartile, and the minimum and

1072 maximum within a range of twice the inter-quartile value.

1073

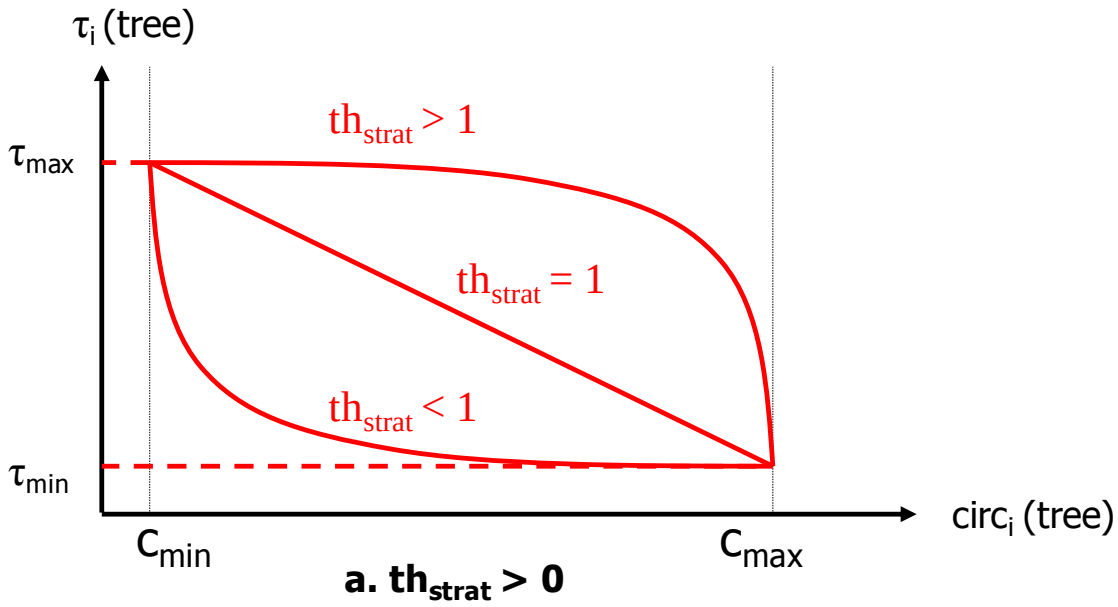

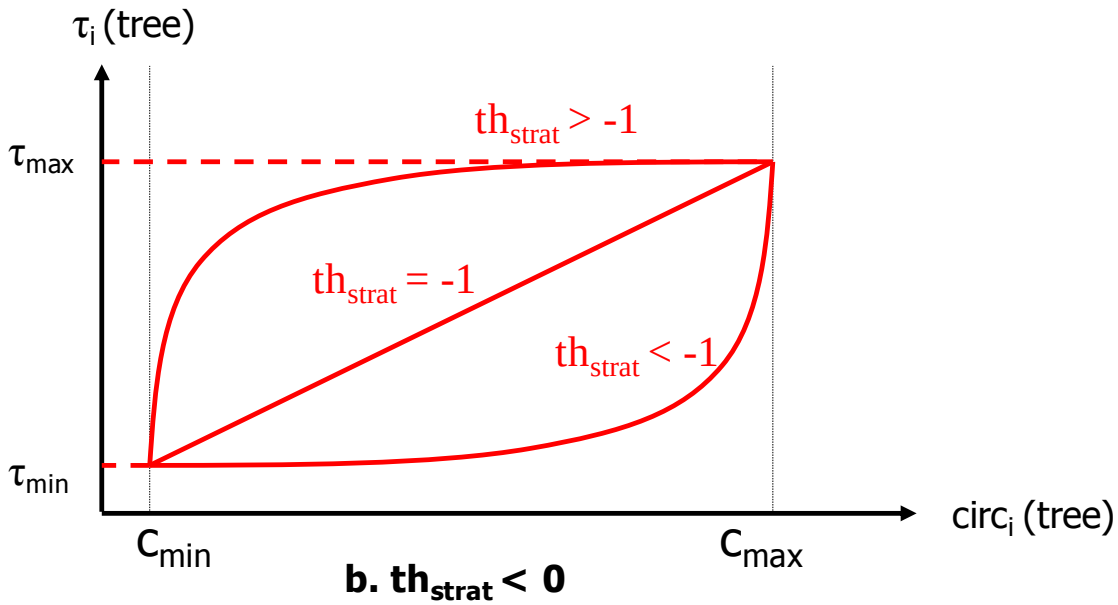

1074

1075 Figure A 4. Thinning strategies as a function of th_{strat}

1076 $circ_i$ is the circumference of tree i, c_{min} and c_{max} are respectively the minimum and

1077 maximum tree circumference in the stand, and τ_i is the probability of death of tree i and

1078 τ_{min} and τ_{max} are respectively the minimum and maximum probabilities of death in the

1079 stand. For th_{strat}, see Eq. 12.

1080

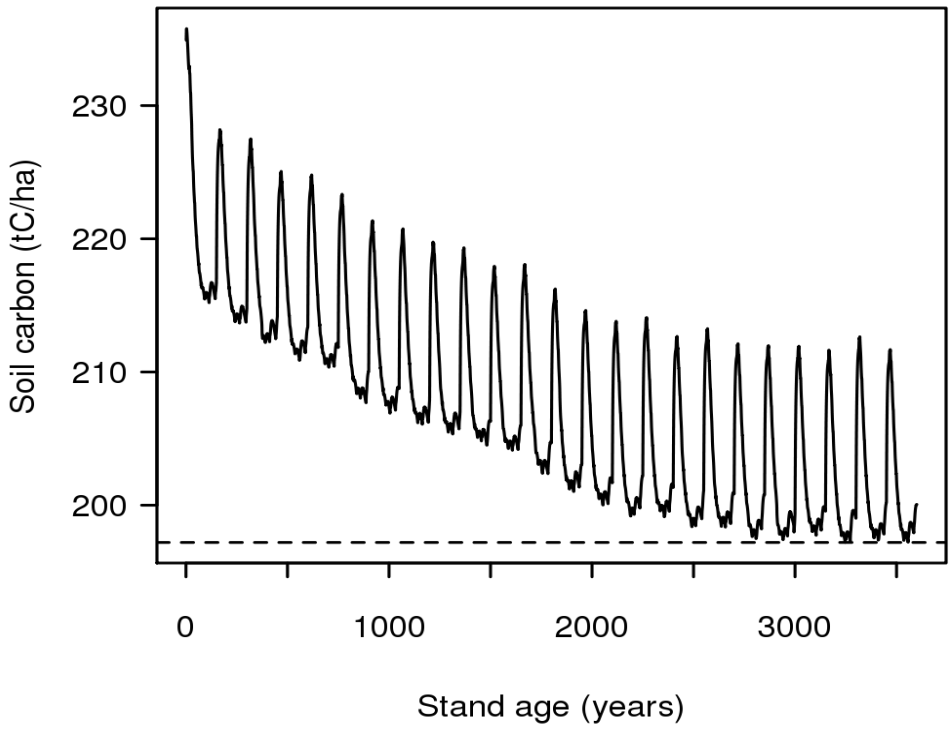

1081

1082 Figure A 5. Long-term soil carbon equilibrium

1083

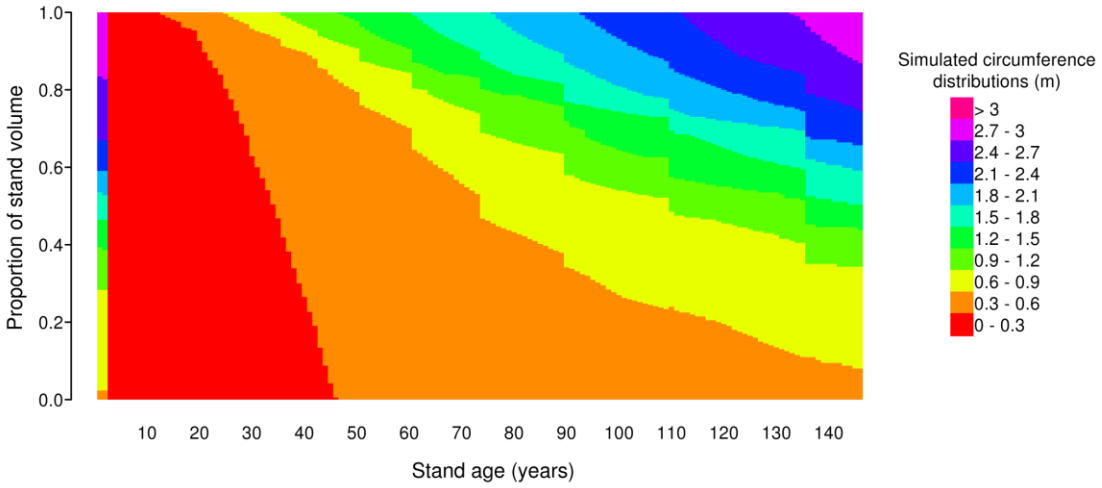

1084

1085 Figure A 6. Evolution of circumference distribution over one forest rotation

1086 One bar represents the simulated distribution of total stand volume between different

1087 tree circumference classes for a given stand age.